

Polarization of gamma-ray burst afterglows in the context of non-axisymmetric structured jets

JIN-DA LI,^{1,2} HE GAO,^{1,2} SHUNKE AI,^{3,4} AND WEI-HUA LEI⁵

¹*Institute for Frontier in Astronomy and Astrophysics, Beijing Normal University, Beijing 102206, China*

²*School of Physics and Astronomy, Beijing Normal University, Beijing 100875, China*

³*Department of Astronomy, School of Physics and Technology, Wuhan University, Wuhan 430072, China*

⁴*Niels Bohr International Academy and DARK, Niels Bohr Institute, University of Copenhagen, Blegdamsvej 17, 2100, Copenhagen, Denmark*

⁵*Department of Astronomy, School of Physics, Huazhong University of Science and Technology, Wuhan, Hubei 430074, China*

ABSTRACT

As the most energetic explosion in the universe, gamma-ray bursts (GRBs) are usually believed to be generated by relativistic jets. Some mechanisms (e.g. internal non-uniform magnetic dissipation processes or the precession of the central engine) may generate asymmetric jet structures, which is characterized by multiple fluctuations in the light curve of afterglow. Since the jet's structure introduces asymmetry in radiation around the line of sight (LOS), it is naturally expected that polarization will be observable. In this work, we reveal the polarization characteristics of gamma-ray burst afterglows with a non-axisymmetric structured jet. Our results show that the afterglow signal generally exhibits polarization, with the degree and evolution influenced by the specific jet structure, observing frequency, and the line of sight (LOS). The polarization degree is notably higher when the LOS is outside the jet. This degree fluctuates over time as different regions of radiation alternate in their dominance, which is accompanied by the rotation of the polarization angle and further reflects the intricate nature of the jet. Regarding its evolution over frequency, the polarization degree displays significant fluctuations at spectral breaks, with the polarization angle possibly undergoing abrupt changes. These features may provide strong evidence for future identification of potential GRBs with asymmetric jet structures.

Keywords: Gamma-ray bursts (629)

1. INTRODUCTION

Gamma-ray bursts are considered to be a kind of catastrophic stellar scale event located at cosmological distances (Zhang 2018). Its energetic radiation suggests catastrophic astrophysical events, typically related to the core collapse of massive stars (Woosley 1993; Paczyński 1998; MacFadyen & Woosley 1999; Woosley & Bloom 2006) or the mergers of two compact stellar objects (neutron star–neutron star and neutron star–black hole binaries) (Paczynski 1986; Eichler et al. 1989; Paczyński 1991; Paczynski 1991; Narayan et al. 1992; Abbott et al. 2017). It is well established that the GRBs are driven by a ultrarelativistic jet from a central engine (neutron stars or black holes). The dissipation of magnetic or kinetic energy in the jet drives the prompt emission a GRB (Rees & Meszaros 1994; Mészáros & Rees 1997; Zhang & Yan 2011), and the interaction between the jet and the interstellar medium provides a long-lasting multi-wavelength afterglow emission (Gao et al. 2013, for a review). The main radiation mechanisms that produce the afterglow signal are synchrotron radiation (which dominates the radiation from radio to X-ray bands) and synchrotron self-Compton scattering radiation (which dominates the radiation in the high-energy gamma-ray band). Since both of these radiation mechanisms inherently produce highly polarized signals, there has been a long history of research on the polarization of gamma-ray burst afterglows.

Medvedev & Loeb (1999) have discussed a process of magnetic field generation and geometric structure, suggesting that the magnetic field is completely tangled in the front plane of shock, but has high coherence in the orthogonal

direction. In this case, polarization can only be observed when the emission region is asymmetrical relative to the observer's line of sight (LOS) (Ghisellini & Lazzati 1999). The polarization properties have been studied when the LOS is not observed along the symmetry axis of the jet (Sari 1999; Ghisellini & Lazzati 1999; Rossi et al. 2004). Here one assumed that the angle between the LOS and the axis of the jet is θ_{obs} , the half angle of the jet is θ_j , and the Lorentz factor of the jet is γ . As long as $1/\gamma > \theta_j - \theta_{\text{obs}}$, the emission region is asymmetric for the observer. In this case, the degree of polarization can achieve 10% approximately, and the polarization direction can only be parallel or perpendicular to the plane where the LOS and jet axis are located (Ghisellini & Lazzati 1999). It should be noted that in this case, the equal arrival time surface (EATS) effect may affect the polarization results, especially in the case of off-axis observations (Huang et al. 2007; Lan et al. 2023).

The asymmetric distribution of the radiation region around the LOS caused by the jet structure can also result in obvious polarization characteristics of the afterglow signal. Rossi et al. (2004) have discussed the polarization properties of power-law and Gaussian jets. They found that the evolution of polarization is sensitive to the luminosity distribution of the jet. For power-law jets, the time at which polarization peaks aligns with the break of light curve, which contrasts with the moment of minimum polarization observed at this moment in homogeneous jets. On the other hand, the exponential wings of the Gaussian jets shift the peak time of polarization after the break in the light curve. Wu et al. (2005) studied the polarization of two-component jets. Its polarization evolution largely depends on the ratio of the intrinsic parameters of the two components, lateral expansion and observation angle. Over a broad range of viewing angle, the narrow component exert a dominant influence on polarization for an extended duration. The common feature of these structures is that they are symmetrical relative to the jet axis, and the possible polarization angle is the same as that of homogeneous jets.

Except for symmetrical structure, some physical processes may generate asymmetric structured jets, e.g. non-uniform magnetic dissipation within the jet, as suggested by Narayan & Kumar (2009) and the precession of central engines in GRBs, as indicated by Huang et al. (2019). More recent work by Lamb et al. (2022) explored 3D hydrodynamic jets in neutron star mergers environment and indeed found some rotational variation of inhomogeneity. Under the framework of asymmetric structures, some models were proposed to explain the prompt emission properties of GRBs, such as the jet hotspots, the patchy shells and the micro/sub jets (Nakamura 2000; Yamazaki et al. 2004; Ioka et al. 2005). On the other hand, Mészáros et al. (1998) noted differences in afterglow due to the angular anisotropy of fireballs. Most recently, Li et al. (2023) conducted a detailed analysis of the potential characteristics of GRB afterglows within the framework of non-axisymmetric structured jets, and they found that radiative contributions from multiple elements may lead to the appearance of multiple distinct peaks or plateaus in the light curve.

Here we will delve into the polarization properties of the afterglow signal generated by the non-axisymmetric jet. We will present the evolution of the degree of polarization and the polarization angle over time at a given observation frequency. Additionally, we will also demonstrate how the degree of polarization and the polarization angle vary with frequency at a given time. Lastly, we will thoroughly examine the impact of different LOS directions on the results.

2. MODEL DESCRIPTION

Li et al. (2023) have established an asymmetric jet modeling method by dividing the jet into N elements and analyzed the afterglow light curve. One can describe the asymmetric jet on the cross-section of the jet using polar coordinates (see Figure 1). The jet axis is set as the coordinate original point, from axis ($\theta = 0$) to the edge of the jet ($\theta = \theta_j$) is the θ direction, and the circumference is φ direction with $\varphi \in [-\pi, \pi]$. The N elements represent the distribution of parameters are step function of φ . Each element can be approximated as a uniform "patch". The angle between LOS and jet axis is θ_{obs} . And the projection's polar angle of the LOS on the jet cross-section is φ_{obs} .

The ejecta of the jet is assumed as a magnetized plasma slab. When viewed perpendicular to the slab, the magnetic field structure appears to be completely tangled. Conversely, when observed parallel to the slab, the magnetic field structure exhibits a certain degree of ordering. Such a magnetic field can be generated through unidirectional compression of a 3-dimensional tangled magnetic field (Laing 1980) or Weibel instability (Medvedev & Loeb 1999). Assuming the degree of polarization observed parallel to the slab is P_0 , at an angle ρ' from the normal of the slab, the polarization can be expressed as (Laing 1980):

$$P(\rho') = \frac{\sin^2 \rho'}{1 + \cos^2 \rho'} P_0. \quad (1)$$

The value of P_0 is determined by the mechanism that produces the photons. For instance, we consider both synchrotron radiation and synchrotron self-Compton scattering in this work. P_0 for synchrotron photons depends on the index of

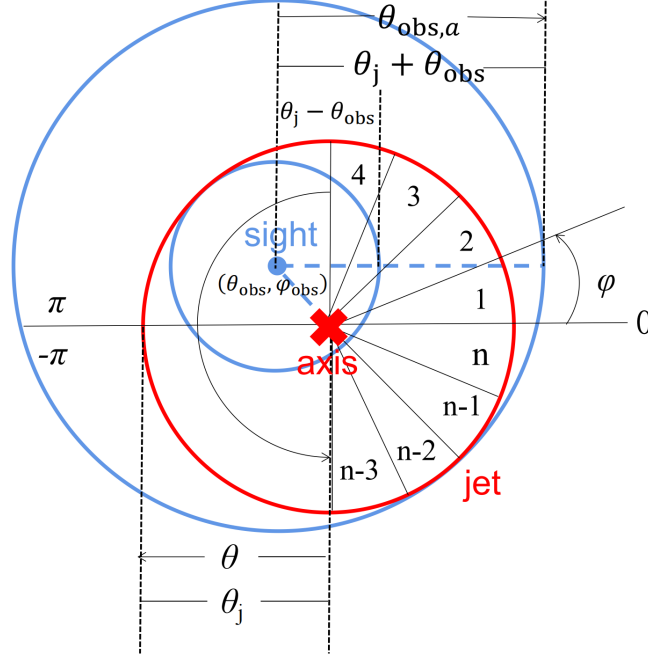


Figure 1. The diagram illustrates the jet structure and coordinate system. The red circle represents the cross-section of a jet with a half opening angle of θ_j . Using the jet axis as the coordinate original point, from axis ($\theta = 0$) to the edge of the jet ($\theta = \theta_j$) is the θ direction, and the circumference is φ direction with $\varphi \in [-\pi, \pi]$. The distribution of physical parameters on the jet circumference are step function of φ , and the cross-section is divided into N elements. The projection of the observer's LOS on the jet cross-section is marked as "sight", and the coordinate is $(\theta_{\text{obs}}, \varphi_{\text{obs}})$. The emission of the jet is the integral of the circles with the radius $(\theta_{\text{obs},a})$ from 0 to $\theta_j + \theta_{\text{obs}}$ around the LOS. For a uniform jet, only the emission between $\theta_j - \theta_{\text{obs}}$ and $\theta_j + \theta_{\text{obs}}$ is polarized.

the power-law distribution of the radiating electrons and can be calculated by averaging over their isotropic distribution (Longair 1994). P_0 for photons originating from SSC scattering is assumed to be 100% (Gill et al. 2020). Since the jet moves in the direction perpendicular to the slab with Lorentz factor γ , the relativistic aberration of photons cannot be ignored. The photons observed at $\rho = 1/\gamma$ in observer's frame correspond to those at $\rho' = \pi/2$ in jet's comoving frame.

For the i -th element, the polarization of each point source on an element with an angle $\theta_{\text{obs},a}$ from the LOS can be written in the complex number field as $\vec{P} = P(\theta'_{\text{obs},a}) e^{2i\theta_p}$ (Ghisellini & Lazzati 1999), where θ_p is the polarization angle of the linear polarization in the observer frame. If the position angle relative to the LOS is set to be χ , then we have $\theta_p = \chi$ for synchrotron radiation (Ghisellini & Lazzati 1999) and $\theta_p = \chi + \pi/2$ for SSC scattering (Gill et al. 2020). All point sources with equal $\theta_{\text{obs},a}$ form a loop around the LOS (see Figure 1). The polarization of the jet at an angle $\theta_{\text{obs},a}$ from the LOS results from the combined contributions of each point source arranged in a ring, which can be expressed as an integral with respect to χ . But only the portion of each loop within the element contributes to the polarization. If the position angle range of the loop within the element is defined as from χ_1 to χ_2 , the polarization of the loop is

$$\vec{P}_i(\theta_{\text{obs},a}) = P_i(\theta'_{\text{obs},a}) \int_{\chi_1}^{\chi_2} e^{2i\theta_p} d\chi. \quad (2)$$

The polarization of the i -th element is the integral over the $\theta_{\text{obs},a}$:

$$\vec{P}_i = \frac{1}{F_{\nu,i}} \int_0^{\theta_j + \theta_{\text{obs}}} F_{\nu,i,a}(\theta_{\text{obs},a}) \vec{P}_i(\theta_{\text{obs},a}) d\theta_{\text{obs},a}. \quad (3)$$

And the polarization of the jet is:

$$\vec{P}_t = \frac{1}{F_{\nu,t}} \int_0^{\theta_j + \theta_{\text{obs}}} \sum_{i=1}^n F_{\nu,i,a}(\theta_{\text{obs},a}) \vec{P}_i(\theta_{\text{obs},a}) d\theta_{\text{obs},a}. \quad (4)$$

The $F_{\nu,t}$ is the total radiation flux of afterglow of the asymmetric jet with N elements, which is the sum of afterglow flux from each element:

$$F_{\nu,t} = \sum_{i=1}^n F_{\nu,i}. \quad (5)$$

The $F_{\nu,i,a}(\theta_{\text{obs},a})$ is the afterglow radiation flux of a loop with radius $\theta_{\text{obs},a}$. And the afterglow radiation flux of the i -th element $F_{\nu,i}$ is the integral of $F_{\nu,i,a}$ over $\theta_{\text{obs},a}$:

$$\begin{aligned} F_{\nu,i} &= \int_0^{\theta_j + \theta_{\text{obs}}} F_{\nu,i,a}(\theta_{\text{obs},a}) d\theta_{\text{obs},a} \\ &= \int_0^{\theta_j + \theta_{\text{obs}}} F_{\nu,a}(\theta_{\text{obs},a}) \chi_i(\theta_{\text{obs},a}) d\theta_{\text{obs},a}. \end{aligned} \quad (6)$$

Where $\chi_i(\theta_{\text{obs},a})$ is the total position angle of the loop with $\theta_{\text{obs},a}$ in the i -th element, which is the part on a loop that contributes to the radiation of afterglow. And $F_{\nu,a}$ represents the afterglow radiation flux of a point source on the element with an angle $\theta_{\text{obs},a}$ to LOS. It worth noting that [Lan et al. \(2023\)](#) found the influence of the EATS effect on polarization, the EATS effect shouldn't be ignored. The radiation flux needs to be transferred to the observer direction through Doppler conversion. Therefore, $F_{\nu,a}$ is represented by ([Granot et al. 2002](#))

$$F_{\nu,a} = a^3 F_{\nu/a}(at), \quad (7)$$

with a factor

$$a = \frac{1 - \beta}{1 - \beta \cos \theta_{\text{obs},a}} \approx \frac{1}{1 + \gamma^2 \theta_{\text{obs},a}^2}, \quad (8)$$

where $F_{\nu}(t)$ is the flux at $\theta_{\text{obs},a} = 0$ along the observer time t of the point source. It is related to the physical properties of the element and the electrons in the interstellar medium. The formulae for calculating the specific flux F_{ν} for synchrotron radiation and SSC scattering are detailed in Appendix.

3. POLARIZATION PROPERTIES FOR A NON-AXISYMMETRIC JET

With the formula introduced in Section 2, here we show the polarization properties for a non-axisymmetric jet in some specific cases. In this section, we only present the results of jets decelerating in uniform interstellar medium.

3.1. Asymmetric Jet With 2 Elements

The simplest asymmetric jet structure is characterized by a sharp interface between two distinct elements resulting from variations of the physical parameters γ_0 and E_{iso} at different azimuth φ . The interface between two elements is defined as $\varphi = 0$ or $\varphi = \pm\pi$. Following [Li et al. \(2023\)](#), we describe this structure as:

$$\gamma_0 = \begin{cases} \gamma_{0,1} & 0 < \varphi < \pi, \\ \gamma_{0,2} & \text{others,} \end{cases} \quad (9)$$

and

$$E_{\text{iso}} = \begin{cases} E_{\text{iso},1} & 0 < \varphi < \pi, \\ E_{\text{iso},2} & \text{others.} \end{cases} \quad (10)$$

Figure 2 shows the cross section for the asymmetric jet.

The afterglow light curves and the evolution of polarization degree and polarization angle of the asymmetric jets with 2 elements are shown in Figure 3, 4 and 5. In the examples, we set $\gamma_{0,1} = 300$, $\gamma_{0,2} = 150$, $E_{\text{iso},1} = 10^{51}$ ergs, $E_{\text{iso},2} = 10^{52}$ ergs for Figure 3. In order to compare the asymmetric jets with different parameters, we set the $E_{\text{iso},2} = 10^{53}$ ergs for Figure 4 and $\gamma_{0,2} = 60$ for Figure 5. For each case, the relative position between the LOS and the jet can be divided into three situations: (1) $\varphi = 0$, the LOS being through the plane of the interface; (2) $\varphi > 0$, the LOS leaning towards the first element; (3) $\varphi < 0$, the LOS leaning towards the second element. Specifically, we fix the half-opening angle $\theta_j = 5^\circ$. And we compare the polarization at different angle between LOS and jet axis $\theta_{\text{obs}} = 0.25\theta_j, 0.5\theta_j, 1.25\theta_j$ and $1.5\theta_j$, respectively. We set other parameters related to the forward shock as: the fractions of the total shock-generated

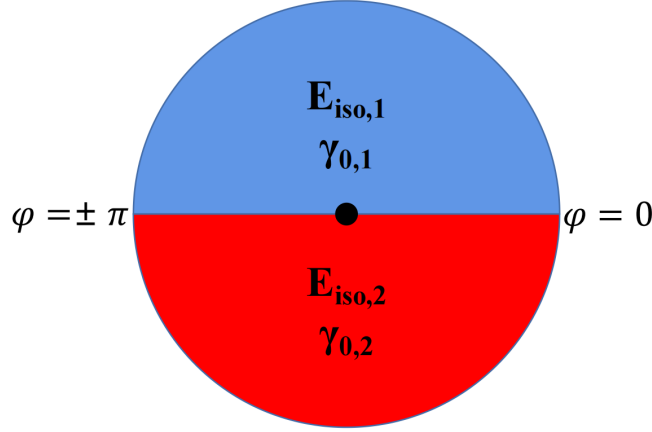


Figure 2. Schematic diagram of a asymmetric jet’s cross-section with 2 elements. The interface between 2 elements local at $\varphi = 0$ or $\varphi = \pm\pi$.

internal energy that goes into the random magnetic field $\epsilon_B = 0.001$ and into the electrons $\epsilon_e = 0.01$; particle number density of interstellar medium $n = 10 \text{ cm}^{-3}$; the power-law distribution index of electrons $p = 2.7$; the red shift $z = 1$ and the degree of polarization observed parallelly $P_0 = 60\%$ for synchrotron radiation. As an example, we consider an observation frequency of $\nu_{\text{obs}} = 8.22 \times 10^{14} \text{ Hz}$ for all the calculations of temporal evolution.

Our results suggest that for the asymmetric jets with 2 elements, polarization is generally present in the afterglow signal observed at most LOS, except for the direction along the jet axis. And the specific polarization evolution depends on the physical parameters of these two elements and the relative position between the jet and LOS. The element that dominate radiation can also dominate polarization evolution.

As shown in Figure 3, overall, the polarization degree of the signal is significantly higher when the observation direction is off-axis compared to when the LOS is within the jet. For the latter case, the afterglow signal shows significant polarization at the late stage corresponding to the peak of the slower-moving component radiation, with a maximum polarization degree of up to 20% when the LOS tends towards the faster-moving component. On the contrary, when the LOS tends towards the slower-moving component, the polarization may be observed with a maximum polarization degree of about 10%, which occurs later than when the LOS tends towards the faster-moving component. For the comparison of the cases with $\varphi_{\text{obs}} = \pm\pi/4$, when $\varphi_{\text{obs}} = \pi/4$, the maximum polarization degree corresponding to $\theta_{\text{obs}} = 0.25\theta_j$ occurs at $t \sim 320\text{s}$, while the maximum polarization degree corresponding to $\theta_{\text{obs}} = 0.5\theta_j$ occurs at $t \sim 1600\text{s}$, with both maximum polarization degrees being approximately 25%. Conversely, when $\varphi_{\text{obs}} = \pi/4$, regardless of whether $\theta_{\text{obs}} = 0.25\theta_j$ or $\theta_{\text{obs}} = 0.5\theta_j$, their maximum polarization degrees occur after 10^4s and are both below 10%. In this case, when the LOS is perpendicular to the boundary between the faster- and slower-moving components (e.g. $\varphi_{\text{obs}} = \pm\pi/2$), the polarization angle does not change with time. Otherwise, the polarization angle will gradually rotate towards the direction of the component that is away from LOS after $1/\gamma_1$ or $2 > \theta_{\text{obs}} - \theta_j$. For example, when $\varphi_{\text{obs}} = \pi/4$, the polarization angle for $\theta_{\text{obs}} = 0.25\theta_j$ or $0.5\theta_j$ rotates from approximately 90° to about 60° around 10^4s towards the slower-moving component. In contrast, when $\varphi = -\pi/4$, the polarization angle rotates from approximately 0° to about 15° towards the faster-moving component before 10^4s .

When the LOS falls outside the jet, polarization is present in the early rising phase of the light curve. When the LOS tends towards the slower-moving component, the early polarization can approach 10%, and as the main radiation of the jet gradually enters the LOS, the polarization evolution curve exhibits a peak corresponding to the light curve, with polarization reaching a maximum of 50%. In this case, if the LOS is perpendicular to the boundary between the faster- and slower-moving components, the polarization angle does not change with time. Otherwise, it will keep constant until the peak of the radiation from the slow-moving component, and then gradually rotate towards the direction of the faster-moving component. The polarization evolution for $\varphi_{\text{obs}} = -\pi/4$ and $\theta_{\text{obs}} = 1.25\theta_j$ in Figure 3 serves as a typical example. At $t \sim 10\text{s}$, its polarization degree is about 8%, gradually rising to a maximum polarization degree of approximately 53% by $t \sim 240\text{s}$. The polarization angle remains about 135° before 3000s, after which it gradually rotates to approximately 155° during the decay phase of the afterglow radiation. On the other hand, when the LOS tends towards the faster-moving component or is on the interface of two elements, the early polarization is below 5%, and as the main radiation of both faster- and slower-moving components enters the LOS successively,

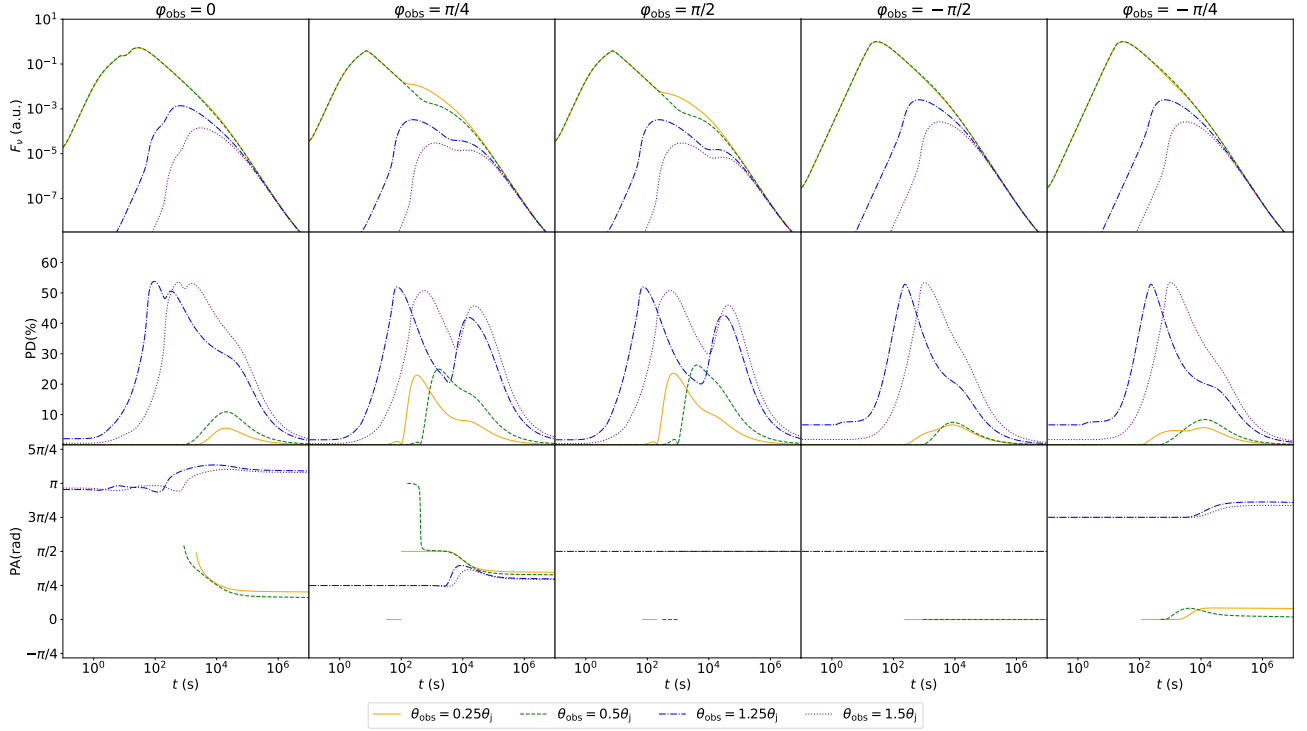


Figure 3. The afterglow light curves (F_ν) and the evolution of polarization degree (PD) and angle (PA) of the asymmetric jets with 2 elements at $\nu = 8.22 \times 10^{14}$ Hz. Polarization is only sensitive to the evolution of the light curve, so the flux of afterglow radiation has been normalized. Considering that low polarization degree is difficult to observe, we only show the polarization angle evolution when the polarization is significant. Generally, the range of polarization angle is $[0, \pi]$, but for the continuity of the polarization angle evolution curve, the range of the coordinate axis is extended. We set the Lorentz factors and the equivalent isotropic energy of the two elements as $\gamma_{0,1} = 300$, $E_{\text{iso},1} = 10^{51}$ ergs and $\gamma_{0,2} = 150$, $E_{\text{iso},2} = 10^{52}$ ergs, respectively. The relative position between the observer and the jet can be divided into three situations: (1) $\varphi = 0$, the LOS through the plane of the interface; (2) $\varphi > 0$ represent the LOS leans towards the first element; (3) $\varphi < 0$ represent the LOS leans towards the second element. And different colors distinguish different θ_{obs} . Other parameters: $\theta_j = 5^\circ$, $\epsilon_e = 0.01$, $\epsilon_B = 0.001$, $p = 2.7$, $n = 10 \text{ cm}^{-3}$, $z = 1$, $P_0 = 60\%$.

two peaks corresponding to the light curve appear on the polarization evolution curves, with the first higher peak reaching a maximum polarization of about 50%. Afterwards, the second lower peak reaching a maximum polarization of about 40%. In these cases, again the polarization angle does not change with time when $|\varphi_{\text{obs}}| = \pi/2$. Otherwise, it will almost keep constant until the peak of the radiation from the faster-moving component, and then gradually rotate towards the direction of the slower-moving component. However, after the slower-moving component dominates the radiation, the polarization angle rotates rapidly in the direction of faster-moving component, until as radiation decreases, the polarization angle gradually rotates again in the direction of the slower-moving component. Taking the polarization evolution for $\varphi_{\text{obs}} = \pi/4$ and $\theta_{\text{obs}} = 1.25\theta_j$ as an example, its polarization degree is approximately 2% at 1s, reaching the first peak of $\sim 52\%$ at about 71s. Following this, the polarization degree gradually declines to a local minimum of about 20%, during which the polarization angle rotates from approximately 45° to about 70° . The polarization degree reaches the second peak of approximately 42% at $t \sim 15700$ s, while the polarization angle simultaneously rotates in the opposite direction to about 55° .

Next, we investigated the impact of increasing the energy ratio and velocity ratio of the two components on the results. As shown in Figure 4, when the energy of the slower-moving component is increased, the re-brightening signature in the light curve becomes more prominent and the signal polarization during the rebrightening signal also increases, regardless of whether the LOS is within the jet or not. Consider the case of $\varphi_{\text{obs}} = 0$ and $\theta_{\text{obs}} = 1.25\theta_j$; in this scenario, the second peak of polarization degree in Figure 3 is lower than the first, while in Figure 4, it is the opposite. The evolution of polarization angle is not sensitive to the changes in energy ratio. As shown in Figure 5, if the velocity ratio of the two components is further increased, the polarization evolution may become more complex. Especially when the LOS tends towards the slower-moving component, for the on-axis case, polarization signals may

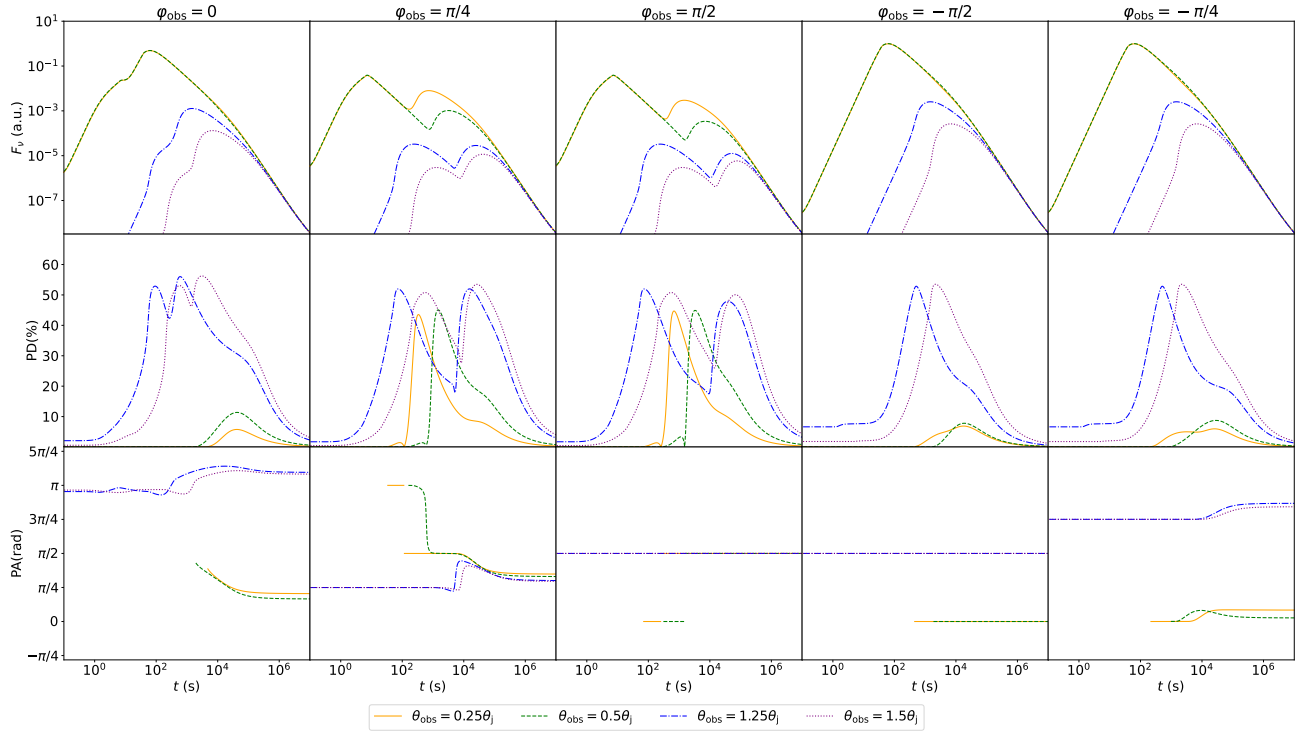


Figure 4. Same to the Figure 3, but the $E_{\text{iso},2} = 10^{53}$ ergs.

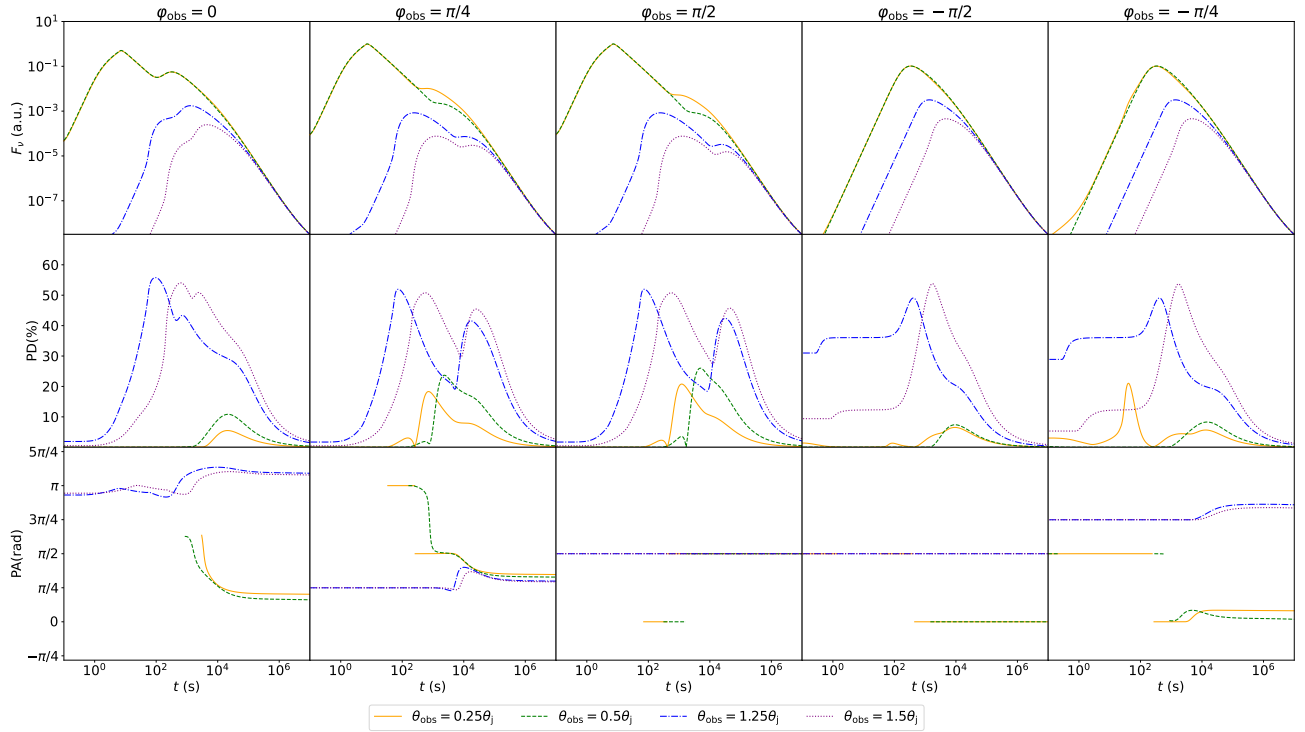


Figure 5. Same to the Figure 3, but the $\gamma_{0,2} = 60$.

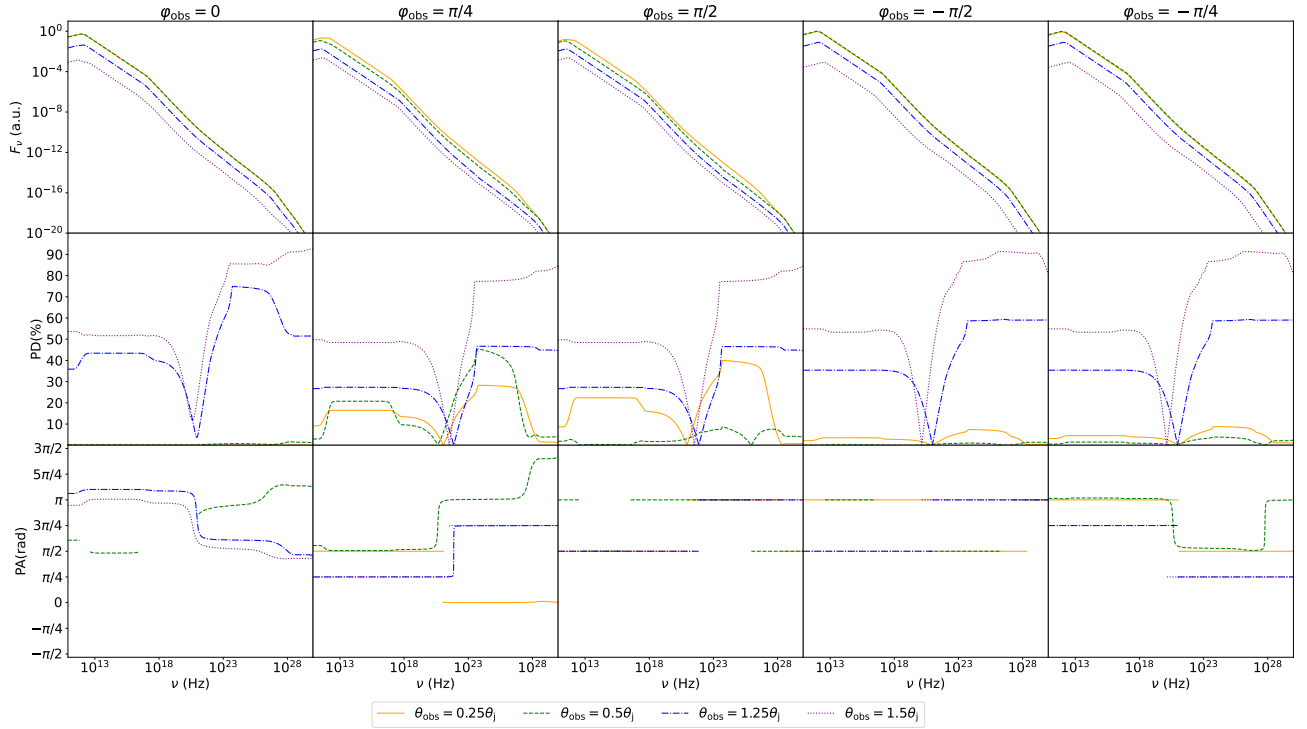


Figure 6. The afterglow spectrum (F_ν) and the spectral distribution of polarization degree (PD) and angle (PA) of the asymmetric jets with 2 elements at $t = 10^3$ s. Polarization is only sensitive to the shape of spectrum, so the flux of afterglow radiation has been normalized. The parameters are same to the Figure 3.

appear during the early rise phase of the light curve, with polarization degrees up to 20%, which is much higher than other on-axis cases at this phase. And the evolution at late-stage polarization are similar to the other cases. As shown in the case of $\varphi_{\text{obs}} = -\pi/4$ and $\theta_{\text{obs}} = 0.25\theta_j$, the maximum polarization degree occurs before the peak of the light curve. For the off-axis case, the polarization degree increases rapidly in the early stages and remains at a relatively high level (e.g. 20% – 40%) until the components enter the LOS. For instance, when $\varphi_{\text{obs}} = -\pi/4$ and $\theta_{\text{obs}} = 1.25\theta_j$, the polarization degree remains at $\sim 40\%$ from ~ 1 s to ~ 100 s. The evolution of polarization angle is similar to the Figure 3.

Besides the temporal evolution, Figure 6 shows the spectral distribution of the afterglow’s flux and polarization at $t = 10^3$ s, utilizing the same set of parameters as in Figure 3. Similar to the Top-Hat jet model, the polarization degree fluctuates at the breaks (characteristic frequencies) of the spectrum, such as ν_m and ν_c . This phenomenon is observed in both synchrotron-dominated and SSC-dominated regimes. However, the fluctuation of polarization degree in the Top-Hat jet scenario is just a few percent, which is caused by the effect of equal-arrive-time surface. In contrast, under the combined influence of the equal-arrive-time surface and the jet’s asymmetric structure, the polarization degree fluctuations of the 2-element jet can exceed 10% in certain cases. Furthermore, as shown in Figure 6, when the line of sight (LOS) lies within the jet, the extent of the polarization degree fluctuation is greater when the LOS is positioned at the faster-moving component ($\varphi_{\text{obs}} > 0$) compared to when it is located at the interface ($\varphi_{\text{obs}} = 0$) or the slower-moving component ($\varphi_{\text{obs}} < 0$). For example, consider the case with $\theta_{\text{obs}} = 0.5\theta_j$. When $\varphi_{\text{obs}} = \pi/4$, the polarization degree initially increases from less than 10% at ν_m (slightly greater than 10^{11} Hz) to approximately 20% at 10^{13} Hz. As the frequency further increases, particularly in the vicinity of ν_c ($\sim 10^{17}$ Hz), the polarization degree decreases from $\sim 20\%$ to $\sim 10\%$. In the frequency range where the polarization is SSC-dominated, having transitioned from being synchrotron-dominated, the polarization range degree decreases from about 30% at 10^{23} Hz to only a few percent at 10^{27} Hz. When $\varphi_{\text{obs}} = -\pi/4$, the polarization degree is close to 0% across the entire spectrum, with the maximum fluctuation being less than 2%. As for the cases that the LOS are outside the jet ($\theta_{\text{obs}} > \theta_j$), the shape of spectral distribution of polarization degree remains similar as those inside the jet. Accordingly, the change in polarization degree at the characteristic frequencies, which could be accompanied by the rotation of polarization angle, may serve

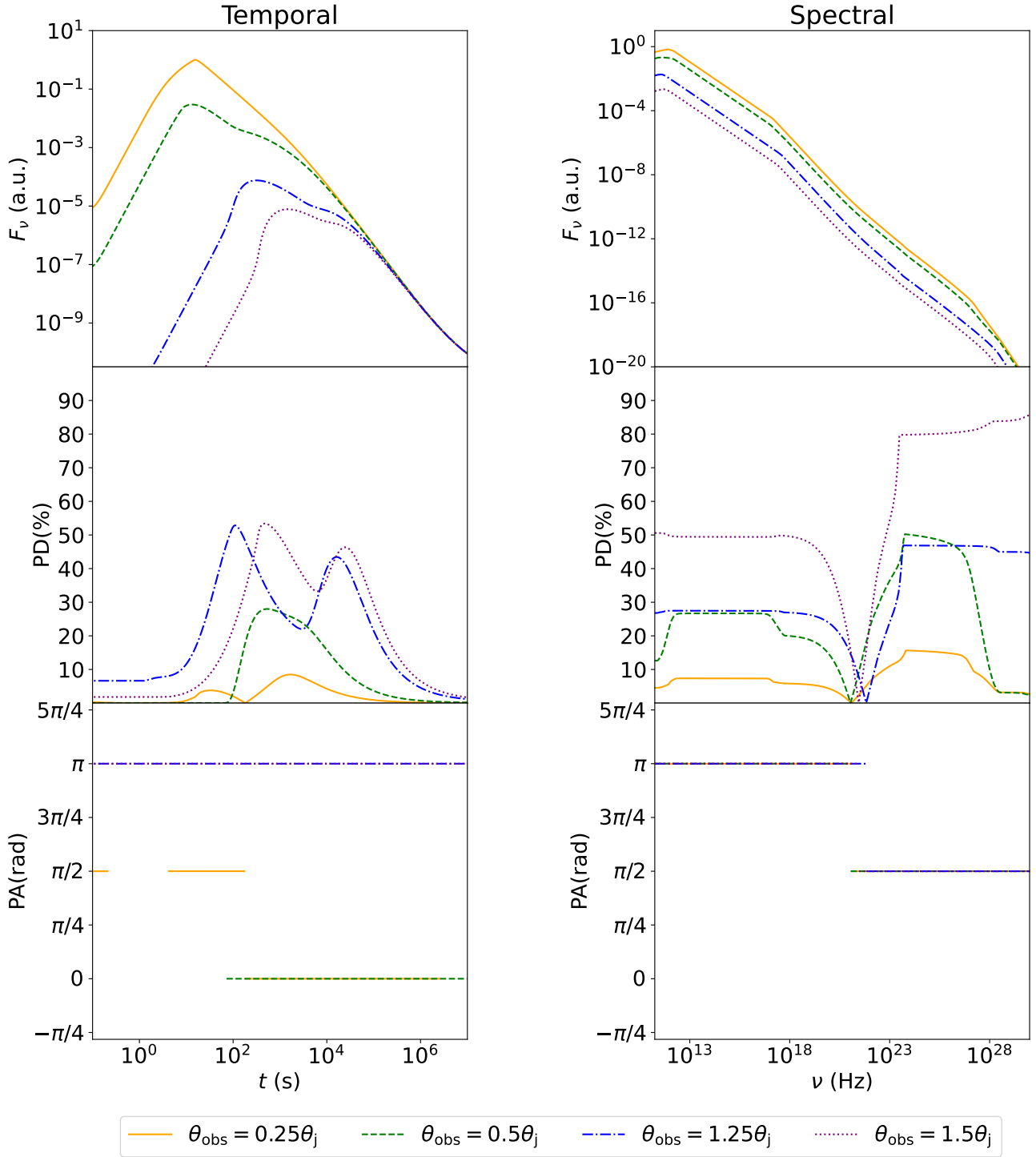


Figure 7. As a comparison, we show the temporal evolution at $\nu = 8.22 \times 10^{14}$ Hz and spectral distribution at $t = 10^3$ s of afterglow and polarization of 2-component jets. We set the Lorentz factor $\gamma_{0,\text{inner}} = 100$ and the equivalent isotropic energy $E_{\text{iso,inner}} = 10^{51}$ ergs for inner component. And $\gamma_{0,\text{outer}} = 50$, $E_{\text{iso,outer}} = 10^{50}$ ergs for outer component. Other parameters are same to the Figure 3

as an important evidence of the existence of a 2-element jet. For example, when $\varphi_{\text{obs}} = \pi/4$ and $\theta_{\text{obs}} = 0.5\theta_j$, the polarization angle rotated by approximately 10° around ν_m .

When the observation frequency exceeds approximately 10^{18} Hz, SSC scattering becomes non-negligible. Due to the disparity in θ_p between synchrotron and SSC emissions (Gill et al. 2020), the polarization degree decreases as the frequency increases, reaching a local minimum at approximately $\sim 10^{21}$ Hz, which accompanied by an intense rotation of the polarization angle by approximately $\pi/2$. Moreover, for all structures of jets, when the observation frequency is higher than the frequency at which the degree of polarization reaches its local minimum, the radiation from SSC dominates the polarization. Since P_0 in SSC scenario is almost 100% in all cases (Gill et al. 2020), its degree of polarization usually achieves a higher level than that of synchrotron radiation. Notably, for the 2-element jet, in most cases, the local minimum of the degree of polarization is $\sim 0\%$, and the polarization angle undergoes a sudden change, similar to that with a Top-Hat jet. However, in certain situations, the local minimum of the polarization degree is $> 0\%$, and the change in the polarization angle is intense but continuous. For example, when $\varphi = 0$ and $\theta_{\text{obs}} = 1.5\theta_j$, the local minimum of the polarization degree is approximately 10%. This phenomenon can be attributed to the influence of the radiation from two asymmetric elements on the symmetry of the radiation area when the LOS approaches the boundary between the two elements.

In previous works, another axisymmetric two-component jet, composed of an inner and an outer part, has often been discussed (e.g. Wu et al. 2005). The inner part consists of a jet with a small opening angle and high velocity, while the outer part consists of a jet with a large opening angle and low velocity. It is of great interest to compare the emission and polarization properties of this jet structure with the non-axisymmetric two-component jet discussed here. We constructed an axisymmetric two-component jet with the following parameters: half-opening angle of outer jet is $\theta_j = 5^\circ$; the half-opening angle of the inner component is $\theta_c = 0.3\theta_j$; the Lorentz factor and equivalent isotropic kinetic energy of the inner component are $\gamma_{0,\text{inner}} = 300$ and $E_{\text{iso,inner}} = 10^{52}$ ergs, respectively; the Lorentz factor and equivalent isotropic kinetic energy of the outer component are $\gamma_{0,\text{outer}} = 150$ and $E_{\text{iso,outer}} = 10^{51}$ ergs. As shown in Figure 7, such a two-component jet also produces rebrightening signature in the light curve. When the LOS is within the jet, the afterglow signal will show significant polarization at the late stage when $1/\gamma_{\text{inner or outer}} > \min(|\theta_c - \theta_{\text{obs}}|, \theta_j - \theta_{\text{obs}})$, with a maximum polarization degree of up to 30%. When the LOS is outside the jet, polarization is present in the early rising phase of the light curve, and the early polarization can be greater than 0%. As the radiation of the outer and inner jet entering the LOS one after another, the polarization evolution curve exhibits two peak corresponding to the light curve, with the polarization reaching a maximum of 50%. In the scenario of axisymmetric two-component jet, the azimuth angle of the LOS direction does not affect the magnitude of the polarization degree, but only determines the specific direction of the polarization angle. Compared to Figure 3, Figure 6 and Figure 7, we find that there is a certain degree of similarity between the light curve and polarization evolution curves of axisymmetric and non-axisymmetric two-component jets. Their spectral distributions of flux and polarization degree are also almost indistinguishable in most cases, except at the frequency where both the contributions of synchrotron and SSC radiations to the polarization are non-negligible. Detecting a local minimum polarization degree that is greater than zero in such cases can provide evidence for the existence of asymmetric structures. In addition, to effectively distinguish between these two structures, monitoring the temporal evolution or spectral distribution of the polarization angle is necessary. For axisymmetric jets, the polarization angle remains in two directions: perpendicular or parallel to the plane of the jet axis and the LOS, while for non-axisymmetric jets, the polarization angle may exhibit complex changes.

3.2. More than 2 elements in a jet

For more complex asymmetric structures, the jet may be divided into multiple elements with $N > 2$. These individual elements exhibit differences in physical parameters, which may consequently lead to more complex polarization evolution and spectral distribution.

As an example, Figure 8 shows the schematic diagrams of the cross-sections of a asymmetric jets with 3 elements. And based on the different initial Lorentz factors γ_0 and equivalent isotropic kinetic energy E_{iso} of each element, the mathematical expression for their structures are

$$\gamma_0 = \begin{cases} \gamma_{0,1} & 0 < \varphi < \varphi_1, \\ \gamma_{0,2} & \varphi_1 < \varphi < \varphi_2, \\ \gamma_{0,3} & \text{others,} \end{cases} \quad (11)$$

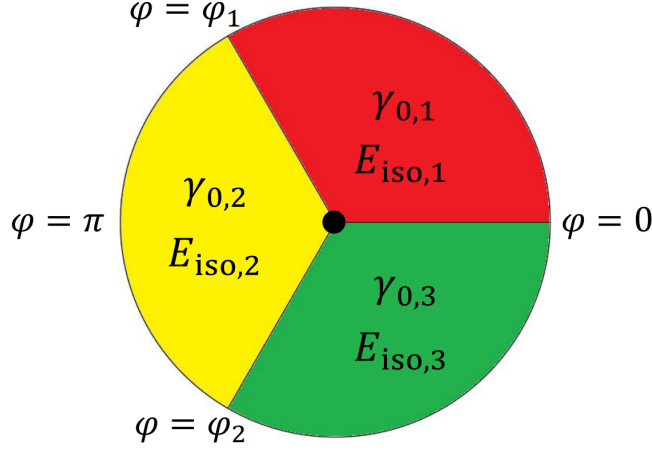


Figure 8. The schematic diagrams of the cross-section of a asymmetric jet with 3 elements. $\varphi = 0, \varphi_1, \varphi_2$ are the interfaces of the jet with 3 elements.

$$E_{\text{iso}} = \begin{cases} E_{\text{iso},1} & 0 < \varphi < \varphi_1, \\ E_{\text{iso},2} & \varphi_1 < \varphi < \varphi_2, \\ E_{\text{iso},3} & \text{others,} \end{cases} \quad (12)$$

for the jet with 3 elements. And the evolution of their corresponding afterglow light curves, polarization degree and polarization angle at $\nu = 8.22 \times 10^{14} \text{Hz}$ are shown in Figure 9. We set $\gamma_{0,1} = 300$, $E_{\text{iso},1} = 10^{51} \text{ergs}$; $\gamma_{0,2} = 150$, $E_{\text{iso},2} = 10^{52} \text{ergs}$; $\gamma_{0,3} = 75$, $E_{\text{iso},3} = 10^{53} \text{ergs}$ for the jet with 3 elements. Other parameters are same to the Figure 3. We considered both the on-axis and off-axis observation, and φ_{obs} ranges from $-\pi$ to π .

The results indicate that for asymmetric jets with $N > 2$ elements, polarization can be observed from any direction. As shown in Figure 9, when the LOS is along the jet axis, the afterglow signal shows a polarized signal from the early stages, and the polarization evolution curve corresponds to fluctuations in the light curve. The polarization degree can reach up to 10%. When the LOS is pointing towards a different direction within the jet, the afterglow signal will show polarization at a later time. The polarization degree evolution curve will also fluctuate corresponding to the evolution of the light curve. The maximum polarization degree can reach 20% – 50%, which is essentially related to the specific parameters (especially the velocity) of the jet element the line of sight falling in.

When the LOS is outside the jet, polarization is present in the early rising phase of the light curve. For the cases whose LOS tends towards the faster-moving components, the early polarization degree is relatively small ($< 10\%$), and there are multiple peaks in the polarization degree evolution curves, with the maximum polarization degree reaching up to 50%. For the cases whose LOS tends towards the slower-moving components, the polarization degree at early time could significantly increase, even up to 30%. In these cases, after maintaining a high level of polarization for a period of time, there may be fluctuations or even higher peaks in the late stage, or it may gradually decay depending on the comparison of different elements' parameters.

For both on-axis and off-axis scenarios, the polarization angle will undergo significant deviation as the radiation intensity of different elements alternate dominance. The speed of polarization angle rotation depends on the difference in parameters between adjacent elements, which essentially reflects the degree of turbulence in the jet structure.

Figure 10 shows the spectral distribution of the afterglow's flux and polarization at $t = 10^3 \text{s}$, for the 3-element jet, utilizing the same set of parameters as in Figure 9. Compare to Figure 6, the rotation of the polarization angle is more pronounced around the characteristic frequency. However, the spectral distributions of both flux and polarization are generally similar to those of the 2-element jet. In rare instances can they be distinctly differentiated from the 2-element jet. For example, when $\varphi_{\text{obs}} = 2\pi/3$ and $\theta_{\text{obs}} = 0.25\theta_j$, in the SSC-dominated bands, the polarization angle shows a persistent variation across the entire frequency range. However, in many cases, such as when $\varphi_{\text{obs}} = \pi/3$ and $\theta_{\text{obs}} = 0.5\theta_j$, the spectral distribution characteristics of the 2-element jet still apply to the 3-element jet. Therefore, the spectral distribution of complex asymmetric structures is often difficult to distinguish from that of 2-element

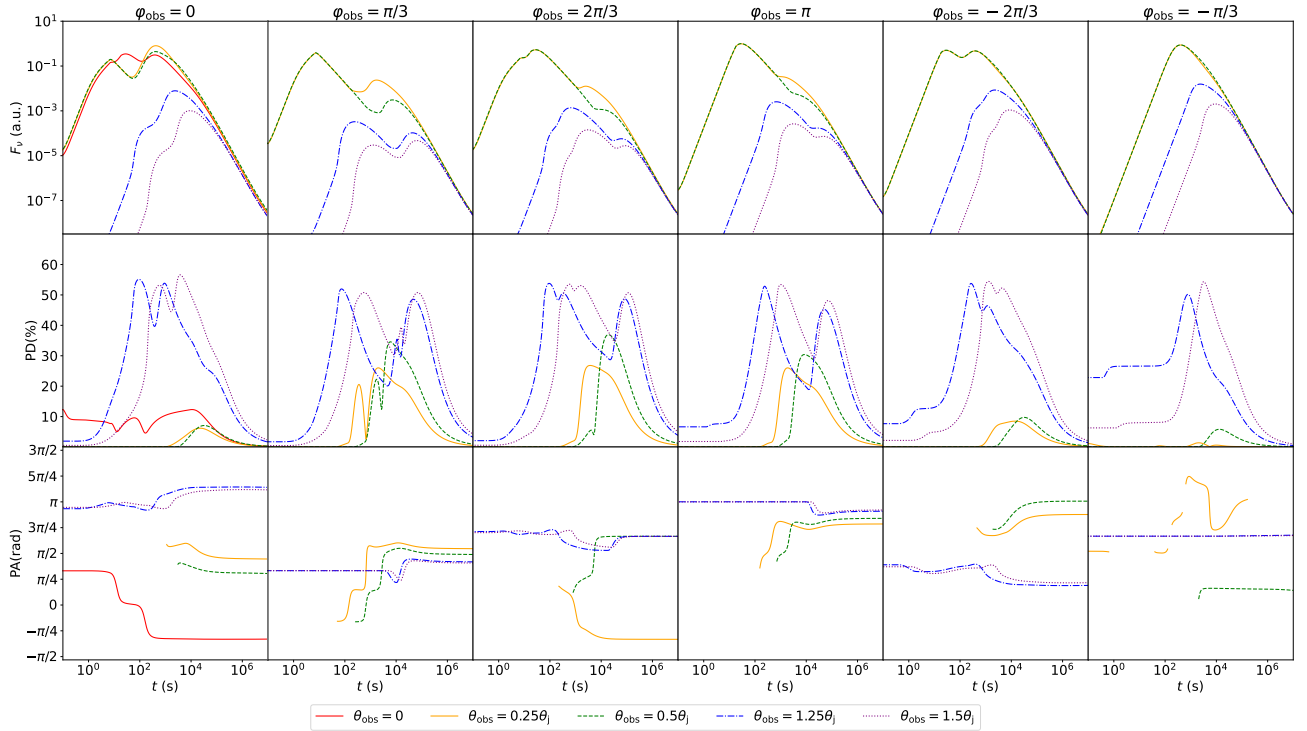


Figure 9. The afterglow light curves (F_ν) and the evolution of polarization degree (PD) and angle (PA) of the asymmetric jets with 3 elements at $\nu = 8.22 \times 10^{14}$ Hz. We show the light curves and polarization evolution in the range from $\varphi_{\text{obs}} = 0$ to $\varphi_{\text{obs}} = 5\pi/3$, and from $\theta_{\text{obs}} = 0$ to $\theta_{\text{obs}} = 1.5\theta_j$. The flux of afterglow radiation has been normalized. The interfaces of the 3 elements are at $\varphi = 0, 2\pi/3$ and $4\pi/3$. The initial Lorentz factor and equivalent isotropic kinetic energy of each element are $\gamma_{0,1} = 100$, $E_{\text{iso},1} = 10^{50}$ ergs; $\gamma_{0,2} = 50$, $E_{\text{iso},2} = 10^{51}$ ergs; $\gamma_{0,3} = 25$, $E_{\text{iso},3} = 10^{52}$ ergs. Other parameters are same to the Figure 3.

jets. This indicates that a more complex asymmetric structure does not necessarily make the spectral distribution of flux and polarization more complex. This is mainly because, in most cases, the afterglow is dominated by a certain element. Radiation from other elements cannot significantly affect the afterglow and polarization. Therefore, to distinguish between different asymmetric structures, it is necessary to monitor the temporal evolution of afterglow and polarization.

In summary, when compared to the situation with 2-elements, there are several points worthy of note when the jet structure is more complex: 1) for the 2-element case, if the LOS is exactly along the jet axis, the polarization degree would be zero. But for multi-element cases, a polarization signal will still appear even $\theta_{\text{obs}} = 0$; 2) the evolution curve of polarization degree and polarization angle will have more fluctuations together with the light curve; 3) the maximum polarization degree, which is around 50%, does not significantly increase due to the complexity of the jet structure. Moreover, due to the similarity in the spectral distribution of flux and polarization among different asymmetric structures, monitoring their temporal evolution is necessary to distinguish between these structures.

4. CONCLUSION AND DISCUSSION

In this work, we analyzed the polarization characteristics of gamma-ray burst afterglows in the context of a non-axisymmetric structured jet, where the jet is divided into N independent and uniform "patch" based on the changes in physical parameters along the azimuth angle (φ) direction. Our results reveal a significant impact of asymmetric structures on polarization evolution and spectral distribution.

The evolution of polarization produced by a non-axisymmetric jet is related to the specific structure of the jet and the direction of the LOS. The polarization degree is generally higher when the LOS is outside the jet than when it is inside the jet. According to the evolution, similar to the characteristics of light curves, the polarization degree also experiences fluctuations as different regions of radiation alternate in dominance, accompanied by gradual rotation of the polarization angle. Relatively low polarization degree and rapid rotation of the polarization angle usually occurs when the contributions of radiation from different regions are competing. Therefore the complexity of the polarization

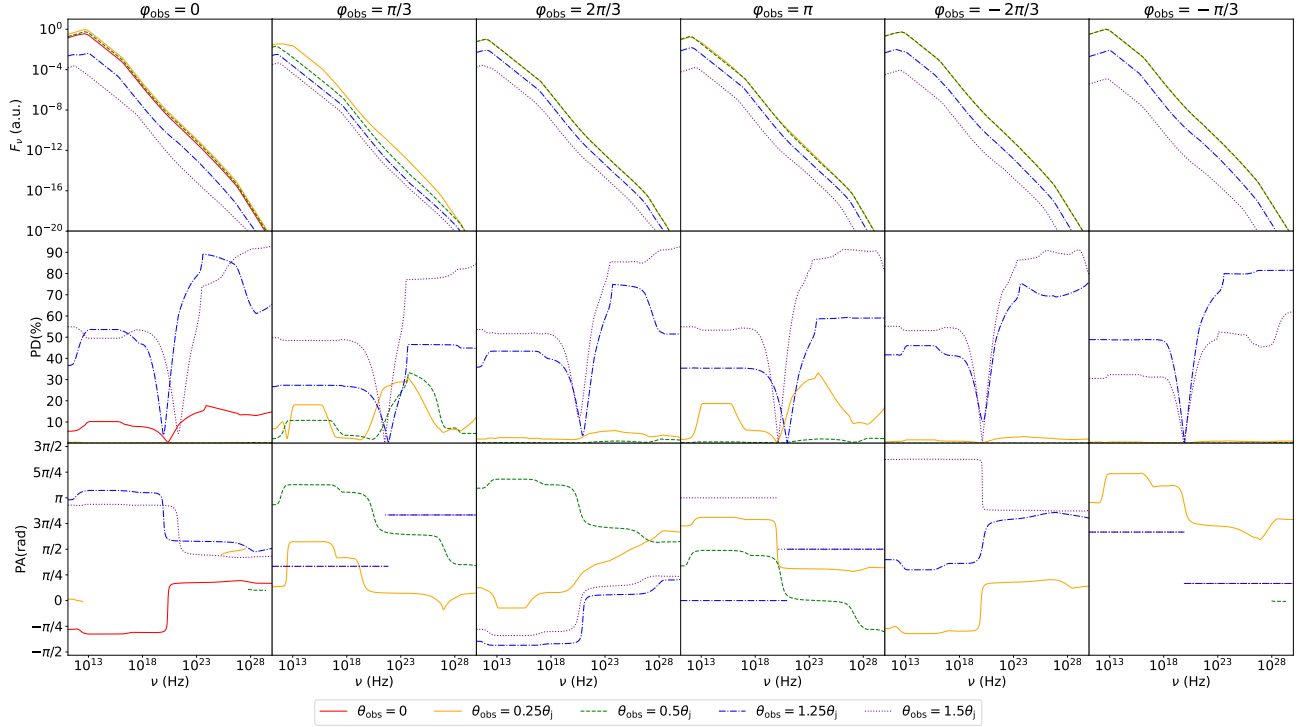


Figure 10. The spectrum (F_ν) and the spectral distribution of polarization degree (PD) and angle (PA) of the asymmetric jets with 3 elements at $t = 10^3$ s. Other parameters are same to the Figure 9.

evolution reflects the complexity of the jet structure. Besides the temporal evolution, the spectral distribution of polarization also emphasizes the influence of the jet structure. For the afterglow produced by a non-axisymmetric jet, the fluctuation in polarization degree at the breaks of the spectrum is greater compared to that of a Top-Hat jet, and it could be accompanied by a rotation of the polarization angle. Additionally, both synchrotron and SSC radiation exhibit significant polarization. However, when the contributions from synchrotron and SSC radiation compete, the polarization degree can be reduced, resulting in a local minimum. The local minimum of the polarization degree generated by symmetric structures is always 0, whereas for asymmetric structures, the local minimum may be non-negligible.

Comparing different asymmetric structures, the polarization and radiation spectral distributions are generally similar. With few exceptions, it is difficult to distinguish different structures based solely on their spectral distribution. However, more complex asymmetric structures exhibit more intricate temporal evolution. Therefore, monitoring the evolution of light curves and polarization curves is more effective for distinguishing between asymmetric jets of varying complexity.

For the spectral distribution of polarization, we did not consider the frequency range below the synchrotron self-absorption frequency (ν_a), where a significant fraction of electrons become thermally distributed. Therefore, the results in the frequency range below ν_a should be modified accordingly (Warren et al. 2018). Mao et al. (2018) have analyzed the impact of relativistic thermal electrons on synchrotron polarization. They found that the large optical depth for radiative transfer results in a low degree of polarization. Future works incorporating the synchrotron self-absorption effect into the framework with a non-axisymmetric jet can aid in studying the jet structure using polarization observations from lower frequencies.

It is worth noting that the specific value of the polarization degree shown in this work is related to the parameter selection used in the examples provided. In real observations, the afterglow signal of different GRBs may exhibit different polarization degrees. However, the evolution of polarization degree and polarization angle shown in this work's results should be universally applicable.

Although it is difficult to observe the polarization of GRBs, many valuable polarization observations have still been achieved so far. For example, the polarization degree of 10.9%, 28% and $< 6\%$ were observed during the early afterglow phase of GRB 090102 (Steele et al. 2009), GRB 120308A (Mundell et al. 2013) and GRB 190829A (Dichiara

et al. 2022), respectively. For the late afterglow phase, the polarization degree of $< 7\%$, 0.27% , 0.8% and 1.2% were observed in GRB 991216 (Granot & Taylor 2005), GRB 171205A (Urata et al. 2019), GRB 190114C (Laskar et al. 2019) and GRB 191221B (Buckley et al. 2021; Urata et al. 2023), respectively. In recent years, with the development of polarization related telescopes and observation technologies, such as POLAR project (Orsi & Polar Collaboration 2011; ORSI 2011), MOPTOP (Shrestha et al. 2020), and MASTER (Lipunov et al. 2019), the polarization of gamma-ray bursts has garnered more attention from researchers. In the future, increased polarization observations of GRB prompt emissions and afterglows will shed light on the mechanisms responsible for their polarization.

Based on observations of the afterglow light curve, it is found that some GRBs do have fluctuations or multiple rebrightening signatures during the late stages (de Wet et al. 2023). Possible explanations for these phenomena include late-stage energy injection, reverse shock or asymmetric structured jets as mentioned here. Since the energy injection process does not significantly affect polarization, the results of this work suggest that polarization detection can effectively distinguish between the two models. And regarding the reverse shock, Lan et al. (2016) have discussed the polarization in scenarios where either the forward shock or the reverse shock dominates. The ordered magnetic field in the reverse shock is markedly different from the tangled magnetic field in the forward shock. Generally, the reverse shock is distinguished by a sudden change in polarization angle at vicinity of the crossing time and after the jet break time. On the other hand, if there is only one significant rebrightening behavior in the late afterglow and it corresponds to a significant polarization degree, it may also be caused by an axisymmetric structured jet (e.g., the two-component jets Huang et al. 2004; Peng et al. 2005; Wu et al. 2005; Beniamini et al. 2020). In this case, the results of this work suggest that the symmetry of the jet structure can be determined by monitoring whether there is a rotation in the polarization angle. Overall, in the future, it is recommended to perform polarimetric observations on GRBs with special features in their late afterglows, in order to ultimately determine the symmetry of the GRB jet structure.

ACKNOWLEDGEMENTS

We appreciate the insightful comments and valuable suggestions from the anonymous referee. This work is supported by the National Natural Science Foundation of China (Projects 12373040, 12021003, U2038107), the National SKA Program of China (2022SKA0130100), the China Postdoctoral Science Foundation (Project 2023M732713), the Fundamental Research Funds for the Central Universities and the Carlsberg Foundation (CF18-0183, PI: I. Tamborra).

REFERENCES

- Abbott, B. P., Abbott, R., Abbott, T. D., et al. 2017, *Phys. Rev. Lett.*, 119, 161101, doi: [10.1103/PhysRevLett.119.161101](https://doi.org/10.1103/PhysRevLett.119.161101)
- Beniamini, P., Granot, J., & Gill, R. 2020, *MNRAS*, 493, 3521, doi: [10.1093/mnras/staa538](https://doi.org/10.1093/mnras/staa538)
- Buckley, D. A. H., Bagnulo, S., Britto, R. J., et al. 2021, *MNRAS*, 506, 4621, doi: [10.1093/mnras/stab1791](https://doi.org/10.1093/mnras/stab1791)
- de Wet, S., Laskar, T., Groot, P. J., et al. 2023, *A&A*, 671, A116, doi: [10.1051/0004-6361/202244917](https://doi.org/10.1051/0004-6361/202244917)
- Dichiara, S., Troja, E., Lipunov, V., et al. 2022, *MNRAS*, 512, 2337, doi: [10.1093/mnras/stac454](https://doi.org/10.1093/mnras/stac454)
- Eichler, D., Livio, M., Piran, T., & Schramm, D. N. 1989, *Nature*, 340, 126, doi: [10.1038/340126a0](https://doi.org/10.1038/340126a0)
- Gao, H., Lei, W.-H., Wu, X.-F., & Zhang, B. 2013, *MNRAS*, 435, 2520, doi: [10.1093/mnras/stt1461](https://doi.org/10.1093/mnras/stt1461)
- Ghisellini, G., Haardt, F., & Svensson, R. 1998, *MNRAS*, 297, 348, doi: [10.1046/j.1365-8711.1998.01442.x](https://doi.org/10.1046/j.1365-8711.1998.01442.x)
- Ghisellini, G., & Lazzati, D. 1999, *MNRAS*, 309, L7, doi: [10.1046/j.1365-8711.1999.03025.x](https://doi.org/10.1046/j.1365-8711.1999.03025.x)
- Gill, R., Granot, J., & Kumar, P. 2020, *MNRAS*, 491, 3343, doi: [10.1093/mnras/stz2976](https://doi.org/10.1093/mnras/stz2976)
- Granot, J., Panaitescu, A., Kumar, P., & Woosley, S. E. 2002, *ApJL*, 570, L61, doi: [10.1086/340991](https://doi.org/10.1086/340991)
- Granot, J., & Taylor, G. B. 2005, *ApJ*, 625, 263, doi: [10.1086/429536](https://doi.org/10.1086/429536)
- Huang, B.-Q., Lin, D.-B., Liu, T., et al. 2019, *MNRAS*, 487, 3214, doi: [10.1093/mnras/stz1426](https://doi.org/10.1093/mnras/stz1426)
- Huang, Y.-f., Dai, Z.-g., & Lu, T. 1999a, *Chinese Physics Letters*, 16, 775, doi: [10.1088/0256-307X/16/10/027](https://doi.org/10.1088/0256-307X/16/10/027)
- Huang, Y. F., Dai, Z. G., & Lu, T. 1999b, *MNRAS*, 309, 513, doi: [10.1046/j.1365-8711.1999.02887.x](https://doi.org/10.1046/j.1365-8711.1999.02887.x)
- Huang, Y. F., Gou, L. J., Dai, Z. G., & Lu, T. 2000, *ApJ*, 543, 90, doi: [10.1086/317076](https://doi.org/10.1086/317076)
- Huang, Y.-F., Lu, Y., Wong, A. Y. L., & Cheng, K. S. 2007, *ChJA&A*, 7, 397, doi: [10.1088/1009-9271/7/3/09](https://doi.org/10.1088/1009-9271/7/3/09)
- Huang, Y. F., Wu, X. F., Dai, Z. G., Ma, H. T., & Lu, T. 2004, *ApJ*, 605, 300, doi: [10.1086/382202](https://doi.org/10.1086/382202)
- Ioka, K., Kobayashi, S., & Zhang, B. 2005, *ApJ*, 631, 429, doi: [10.1086/432567](https://doi.org/10.1086/432567)

- Laing, R. A. 1980, *Monthly Notices of the Royal Astronomical Society*, 193, 439, doi: [10.1093/mnras/193.3.439](https://doi.org/10.1093/mnras/193.3.439)
- Lamb, G. P., Nativi, L., Rosswog, S., et al. 2022, *Universe*, 8, 612, doi: [10.3390/universe8120612](https://doi.org/10.3390/universe8120612)
- Lan, M.-X., Wu, X.-F., & Dai, Z.-G. 2016, *ApJ*, 816, 73, doi: [10.3847/0004-637X/816/2/73](https://doi.org/10.3847/0004-637X/816/2/73)
- . 2023, *ApJ*, 952, 31, doi: [10.3847/1538-4357/acd6ef](https://doi.org/10.3847/1538-4357/acd6ef)
- Laskar, T., Alexander, K. D., Gill, R., et al. 2019, *ApJL*, 878, L26, doi: [10.3847/2041-8213/ab2247](https://doi.org/10.3847/2041-8213/ab2247)
- Li, J.-D., Gao, H., Ai, S., & Lei, W.-H. 2023, *MNRAS*, 525, 6285, doi: [10.1093/mnras/stad2606](https://doi.org/10.1093/mnras/stad2606)
- Lipunov, V. M., Vladimirov, V. V., Gorbovskoi, E. S., et al. 2019, *Astronomy Reports*, 63, 293, doi: [10.1134/S1063772919040073](https://doi.org/10.1134/S1063772919040073)
- Longair, M. S. 1994, *High energy astrophysics. Vol.2: Stars, the galaxy and the interstellar medium, Vol. 2*
- MacFadyen, A. I., & Woosley, S. E. 1999, *ApJ*, 524, 262, doi: [10.1086/307790](https://doi.org/10.1086/307790)
- Mao, J., Covino, S., & Wang, J. 2018, *ApJ*, 860, 153, doi: [10.3847/1538-4357/aac5d9](https://doi.org/10.3847/1538-4357/aac5d9)
- Medvedev, M. V., & Loeb, A. 1999, *ApJ*, 526, 697, doi: [10.1086/308038](https://doi.org/10.1086/308038)
- Mészáros, P., & Rees, M. J. 1997, *ApJL*, 482, L29, doi: [10.1086/310692](https://doi.org/10.1086/310692)
- Mészáros, P., Rees, M. J., & Wijers, R. A. M. J. 1998, *ApJ*, 499, 301, doi: [10.1086/305635](https://doi.org/10.1086/305635)
- Mundell, C. G., Kopač, D., Arnold, D. M., et al. 2013, *Nature*, 504, 119, doi: [10.1038/nature12814](https://doi.org/10.1038/nature12814)
- Nakamura, T. 2000, *ApJL*, 534, L159, doi: [10.1086/312663](https://doi.org/10.1086/312663)
- Nakar, E., Ando, S., & Sari, R. 2009, *ApJ*, 703, 675, doi: [10.1088/0004-637X/703/1/675](https://doi.org/10.1088/0004-637X/703/1/675)
- Narayan, R., & Kumar, P. 2009, *MNRAS*, 394, L117, doi: [10.1111/j.1745-3933.2009.00624.x](https://doi.org/10.1111/j.1745-3933.2009.00624.x)
- Narayan, R., Paczynski, B., & Piran, T. 1992, *ApJL*, 395, L83, doi: [10.1086/186493](https://doi.org/10.1086/186493)
- ORSI, S. 2011, in *International Cosmic Ray Conference, Vol. 6, International Cosmic Ray Conference*, 403, doi: [10.7529/ICRC2011/V06/1128](https://doi.org/10.7529/ICRC2011/V06/1128)
- Orsi, S., & Polar Collaboration. 2011, *Astrophysics and Space Sciences Transactions*, 7, 43, doi: [10.5194/astra-7-43-2011](https://doi.org/10.5194/astra-7-43-2011)
- Paczynski, B. 1986, *ApJL*, 308, L43, doi: [10.1086/184740](https://doi.org/10.1086/184740)
- Paczynski, B. 1991, in *American Institute of Physics Conference Series, Vol. 265, Gamma-ray Bursts*, 144–148, doi: [10.1063/1.42815](https://doi.org/10.1063/1.42815)
- . 1991, *AcA*, 41, 257
- Paczynski, B. 1998, in *American Institute of Physics Conference Series, Vol. 428, Gamma-Ray Bursts, 4th Hunstville Symposium*, ed. C. A. Meegan, R. D. Preece, & T. M. Koshut, 783–787, doi: [10.1063/1.55404](https://doi.org/10.1063/1.55404)
- Peng, F., Königl, A., & Granot, J. 2005, *ApJ*, 626, 966, doi: [10.1086/430045](https://doi.org/10.1086/430045)
- Rees, M. J., & Meszaros, P. 1994, *ApJL*, 430, L93, doi: [10.1086/187446](https://doi.org/10.1086/187446)
- Rossi, E. M., Lazzati, D., Salmonson, J. D., & Ghisellini, G. 2004, *MNRAS*, 354, 86, doi: [10.1111/j.1365-2966.2004.08165.x](https://doi.org/10.1111/j.1365-2966.2004.08165.x)
- Sari, R. 1999, *ApJL*, 524, L43, doi: [10.1086/312294](https://doi.org/10.1086/312294)
- Sari, R., & Esin, A. A. 2001, *ApJ*, 548, 787, doi: [10.1086/319003](https://doi.org/10.1086/319003)
- Sari, R., Piran, T., & Narayan, R. 1998, *ApJL*, 497, L17, doi: [10.1086/311269](https://doi.org/10.1086/311269)
- Shrestha, M., Steele, I. A., Piascik, A. S., et al. 2020, *MNRAS*, 494, 4676, doi: [10.1093/mnras/staa1049](https://doi.org/10.1093/mnras/staa1049)
- Steele, I. A., Mundell, C. G., Smith, R. J., Kobayashi, S., & Guidorzi, C. 2009, *Nature*, 462, 767, doi: [10.1038/nature08590](https://doi.org/10.1038/nature08590)
- Urata, Y., Toma, K., Huang, K., et al. 2019, *ApJL*, 884, L58, doi: [10.3847/2041-8213/ab48f3](https://doi.org/10.3847/2041-8213/ab48f3)
- Urata, Y., Toma, K., Covino, S., et al. 2023, *Nature Astronomy*, 7, 80, doi: [10.1038/s41550-022-01832-7](https://doi.org/10.1038/s41550-022-01832-7)
- Warren, D. C., Barkov, M. V., Ito, H., Nagataki, S., & Laskar, T. 2018, *MNRAS*, 480, 4060, doi: [10.1093/mnras/sty2138](https://doi.org/10.1093/mnras/sty2138)
- Woosley, S. E. 1993, *ApJ*, 405, 273, doi: [10.1086/172359](https://doi.org/10.1086/172359)
- Woosley, S. E., & Bloom, J. S. 2006, *ARA&A*, 44, 507, doi: [10.1146/annurev.astro.43.072103.150558](https://doi.org/10.1146/annurev.astro.43.072103.150558)
- Wu, X. F., Dai, Z. G., Huang, Y. F., & Lu, T. 2003, *MNRAS*, 342, 1131, doi: [10.1046/j.1365-8711.2003.06602.x](https://doi.org/10.1046/j.1365-8711.2003.06602.x)
- . 2005, *MNRAS*, 357, 1197, doi: [10.1111/j.1365-2966.2005.08685.x](https://doi.org/10.1111/j.1365-2966.2005.08685.x)
- Yamazaki, R., Ioka, K., & Nakamura, T. 2004, *ApJL*, 607, L103, doi: [10.1086/421872](https://doi.org/10.1086/421872)
- Zhang, B. 2018, *The Physics of Gamma-Ray Bursts*, doi: [10.1017/9781139226530](https://doi.org/10.1017/9781139226530)
- Zhang, B., & Yan, H. 2011, *ApJ*, 726, 90, doi: [10.1088/0004-637X/726/2/90](https://doi.org/10.1088/0004-637X/726/2/90)

APPENDIX

The polarization of afterglow is sensitive to the shape of the light curve and the spectrum. Li et al. (2023) have developed a method for calculating the afterglow of GRB, which obtains physical parameters at each moment through numerical dynamic evolution and uses these parameters to analytically calculate the radiation flux of afterglow. On the basis of Li et al. (2023), we added SSC radiation and further adjusted the algorithm to make it more suitable for polarization calculation (see Section 2 for details). We refer to the code used in this work as AFGoLipy.

A. SYNCHROTRON RADIATION

In the case of the i -th element shocking the interstellar medium, the characteristic synchrotron frequency of electrons with Lorentz factor $\gamma_e \gg 1$ in magnetic field B in the co-moving frame is (Sari et al. 1998):

$$\nu(\gamma_e) = \gamma_e^2 \frac{q_e B}{2\pi m_e c}, \quad (\text{A1})$$

where m_e , q_e are the mass and charge of a electron, respectively. c is the speed of light. γ is the Lorentz factor of the element's bulk motion, whose evolution can be expressed as (Huang et al. 1999a,b):

$$\frac{d\gamma}{dm} = -\frac{\gamma^2 - 1}{M_{\text{ej}} + \varepsilon m + 2(1 - \varepsilon)\gamma m}, \quad (\text{A2})$$

where $M_{\text{ej}} = E_0/(\gamma_0 c^2)$ is the ejecta mass, and E_0 is the initial kinetic energy of an element. The ε is radiative efficiency, which is defined as the proportion of the internal energy generated by the shock in jet's comoving frame that would be radiated. m is the mass of the interstellar medium swept by the element. If an element occupies the azimuth range from φ_1 to φ_u on the cross-section of the jet, the evolution of m can be written as:

$$\frac{dm}{dR} = (\varphi_u - \varphi_1) R^2 (1 - \cos\theta_j) n m_p, \quad (\text{A3})$$

where m_p is the mass of a proton. n is the particle number density of interstellar medium, which can be described as AR^{-k} , where k is the wind profile variable. And R is the jet's radius. For the uniform interstellar medium, $k = 0$. And for the stellar wind environment, $k = 2$. A is a constant. The evolution of the jet's radius R over time t in the frame of an on-axis observer can reads as:

$$\frac{dR}{dt} = \beta c \gamma (\gamma + \sqrt{\gamma^2 - 1}). \quad (\text{A4})$$

The β represent the dimensionless velocity of the element's bulk motion.

The minimum Lorentz factor for the random motion of electrons can be derived as (Huang et al. 2000)

$$\gamma_{e,\text{min}} = \epsilon_e (\gamma - 1) \frac{m_p (p - 2)}{m_e (p - 1)} + 1, \quad (\text{A5})$$

where ϵ_e is the fraction of the total shock generated internal energy goes into the electrons. p represents the power-law distribution index of electrons in interstellar media ($dN_e/d\gamma_e \propto \gamma_e^{-p}$). And the characteristic Lorentz factor γ_c is defined as (Sari et al. 1998):

$$\gamma_c = \frac{6\pi m_e c}{\sigma_T B^2 t} = \frac{3m_e}{16\epsilon_B \sigma_T m_p c t \gamma^3 n}, \quad (\text{A6})$$

beyond which the electrons might have significantly cooled. Where σ_T is the the cross section for Thompson scattering. If the Synchrotron Self-Compton (SSC) scattering is significant, the cooling of electrons is enhanced. Therefore the γ_c should to be divided by $(1 + Y)$, where Y is the Compton y -parameter. The $\gamma_{e,\text{min}}$, γ_c defines the characteristic frequencies ν_m and ν_c , which divide afterglow radiation into two situations: $\nu_m > \nu_c$ for fast cooling and $\nu_m < \nu_c$ for slow cooling.

In an $n = AR^{-k}$ environment, for the slow cooling regime ($\nu_c > \nu_m$), the self absorption frequency ν_a is

$$\nu_a = \begin{cases} \left[\frac{c_1 q_e n R}{(3-k) B \gamma_c^5} \right]^{3/5} \nu_m & \nu_a < \nu_m, \\ \left[\frac{c_2 q_e n R}{(3-k) B \gamma_c^5} \right]^{2/(p+4)} \nu_m & \nu_m < \nu_a < \nu_c, \\ \left[\frac{c_2 q_e n R}{(3-k) B \gamma_c^5} \right]^{2/(p+5)} \left(\frac{\nu_c}{\nu_m} \right)^{1/(p+5)} \nu_m & \nu_c < \nu_a. \end{cases} \quad (\text{A7})$$

c_1 and c_2 are coefficients dependent on p (Wu et al. 2003). Assuming a point source of the element is on the LOS, the observed flux density F_ν is divided into the following three situations

(1) $\nu_a < \nu_m < \nu_c$:

$$F_\nu^{\text{syn}} = \frac{1}{\Omega} F_{\nu, \text{max}} \begin{cases} \left(\frac{\nu}{\nu_a} \right)^2 \left(\frac{\nu_a}{\nu_m} \right)^{1/3} & \nu < \nu_a, \\ \left(\frac{\nu}{\nu_m} \right)^{1/3} & \nu_a < \nu < \nu_m, \\ \left(\frac{\nu}{\nu_m} \right)^{-(p-1)/2} F_{\nu, \text{max}} & \nu_m < \nu < \nu_c, \\ \left(\frac{\nu}{\nu_m} \right)^{-(p-1)/2} \left(\frac{\nu}{\nu_c} \right)^{-p/2} & \nu_c < \nu < \nu_M. \end{cases} \quad (\text{A8})$$

(2) $\nu_m < \nu_a < \nu_c$:

$$F_\nu^{\text{syn}} = \frac{1}{\Omega} F_{\nu, \text{max}} \begin{cases} \left(\frac{\nu}{\nu_m} \right)^2 \left(\frac{\nu_m}{\nu_a} \right)^{(p+4)/2} F_{\nu, \text{max}} & \nu < \nu_m, \\ \left(\frac{\nu}{\nu_a} \right)^{5/2} \left(\frac{\nu_a}{\nu_m} \right)^{-(p-1)/2} F_{\nu, \text{max}} & \nu_m < \nu < \nu_a, \\ \left(\frac{\nu}{\nu_m} \right)^{-(p-1)/2} F_{\nu, \text{max}} & \nu_a < \nu < \nu_c, \\ \left(\frac{\nu}{\nu_m} \right)^{-(p-1)/2} \left(\frac{\nu}{\nu_c} \right)^{-p/2} F_{\nu, \text{max}} & \nu_c < \nu < \nu_M. \end{cases} \quad (\text{A9})$$

(3) $\nu_m < \nu_c < \nu_a$:

$$F_\nu^{\text{syn}} = \frac{1}{\Omega} F_{\nu, \text{max}} \begin{cases} \left(\frac{\nu}{\nu_m} \right)^2 \left(\frac{\nu_m}{\nu_a} \right)^{(p+4)/2} \left(\frac{\nu_a}{\nu_c} \right)^{-1/2} & \nu < \nu_m, \\ \left(\frac{\nu}{\nu_a} \right)^{5/2} \left(\frac{\nu_a}{\nu_c} \right)^{-p/2} \left(\frac{\nu_c}{\nu_m} \right)^{-(p-1)/2} & \nu_m < \nu < \nu_a, \\ \left(\frac{\nu}{\nu_c} \right)^{-p/2} \left(\frac{\nu_c}{\nu_m} \right)^{-(p-1)/2} & \nu_a < \nu < \nu_M. \end{cases} \quad (\text{A10})$$

where $F_{\nu, \text{max}}$ stands for the peak flux density of the spectrum. ν_M is the maximum frequency of synchrotron radiation, which is defined by the maximum Lorentz factor of electrons γ_M . The parameter Ω is the solid angle of the beaming cone of radiation due to the relativistic beaming effect of the point source, which can be expressed as $\Omega = 2\pi [1 - \cos(1/\gamma)]$, where $1/\gamma$ is the half-opening angle of the beaming cone. To obtain the flux from the point source, introducing the factor $1/\Omega$ is necessary. Incidentally, although the polarization below the synchrotron self-absorption frequency is suppressed, we still present the radiation flux below this frequency for the sake of completeness. In the fast cooling regime ($\nu_c < \nu_m$), the self absorption frequency ν_a is:

$$\nu_a = \begin{cases} \left[\frac{c_1 q_e n R}{(3-k) B \gamma_c^5} \right]^{3/5} \nu_c & \nu_a < \nu_c, \\ \left[\frac{c_2 q_e n R}{(3-k) B \gamma_c^5} \right]^{1/3} \nu_c & \nu_c < \nu_a < \nu_m, \\ \left[\frac{c_2 q_e n R}{(3-k) B \gamma_c^5} \right]^{2/(p+5)} \left(\frac{\nu_m}{\nu_c} \right)^{(p-1)/(p+5)} \nu_c & \nu_m < \nu_a. \end{cases} \quad (\text{A11})$$

And the flux in fast cooling regime is

(1) $\nu_a < \nu_c < \nu_m$:

$$F_\nu^{\text{syn}} = \frac{1}{\Omega} F_{\nu, \text{max}} \begin{cases} \left(\frac{\nu}{\nu_a} \right)^2 \left(\frac{\nu_a}{\nu_c} \right)^{1/3} & \nu < \nu_a, \\ \left(\frac{\nu}{\nu_c} \right)^{1/3} & \nu_a < \nu < \nu_c, \\ \left(\frac{\nu}{\nu_c} \right)^{-1/2} & \nu_c < \nu < \nu_m, \\ \left(\frac{\nu_m}{\nu_c} \right)^{-1/2} \left(\frac{\nu}{\nu_m} \right)^{-p/2} & \nu_m < \nu < \nu_M. \end{cases} \quad (\text{A12})$$

(2) $\nu_c < \nu_a < \nu_m$:

$$F_\nu^{\text{syn}} = \frac{1}{\Omega} F_{\nu, \text{max}} \begin{cases} \left(\frac{\nu}{\nu_c}\right)^2 \left(\frac{\nu_c}{\nu_a}\right)^3 & \nu < \nu_c, \\ \left(\frac{\nu}{\nu_a}\right)^{5/2} \left(\frac{\nu_a}{\nu_c}\right)^{-1/2} & \nu_c < \nu < \nu_a, \\ \left(\frac{\nu}{\nu_c}\right)^{-1/2} & \nu_a < \nu < \nu_m, \\ \left(\frac{\nu_m}{\nu_c}\right)^{-1/2} \left(\frac{\nu}{\nu_m}\right)^{-p/2} & \nu_m < \nu < \nu_M. \end{cases} \quad (\text{A13})$$

(3) $\nu_c < \nu_m < \nu_a$:

$$F_\nu^{\text{syn}} = \frac{1}{\Omega} F_{\nu, \text{max}} \begin{cases} \left(\frac{\nu}{\nu_c}\right)^2 \left(\frac{\nu_c}{\nu_a}\right)^3 \left(\frac{\nu_a}{\nu_m}\right)^{-(p-1)/2} & \nu < \nu_c, \\ \left(\frac{\nu}{\nu_a}\right)^{5/2} \left(\frac{\nu_a}{\nu_m}\right)^{-p/2} \left(\frac{\nu_m}{\nu_c}\right)^{-1/2} & \nu_c < \nu < \nu_a, \\ \left(\frac{\nu}{\nu_m}\right)^{-p/2} \left(\frac{\nu_m}{\nu_c}\right)^{-1/2} & \nu_a < \nu < \nu_M. \end{cases} \quad (\text{A14})$$

It is worth noting that in cases of strong synchrotron self-absorption regime ($\max(\nu_m, \nu_c) < \nu_a$), the dynamical evolution may be influenced by synchrotron self-absorption. For example, the energy distribution of electrons may be closer to a Maxwellian distribution rather than a power-law distribution (Ghisellini et al. 1998). Therefore, readers should apply the above equations with caution when dealing with strong synchrotron self-absorption regime.

B. SYNCHROTRON SELF-COMPTON SCATTERING

The characteristic frequencies of SSC emission are defined by the different combination of the characteristic frequencies ν_a, ν_m, ν_c and characteristic Lorentz factor $\gamma_a, \gamma_m, \gamma_c$ of synchrotron radiation (Sari & Esin 2001). It is convenient for us to define the characteristic frequencies as

$$\nu_{ij}^{\text{IC}} = 4\gamma_i^2 \nu_j x_0, \quad (\text{B15})$$

with the subscripts $i, j = a, c, m$. The characteristic frequencies represent the characteristic upscattered frequency for mono-energetic photons with frequency ν_j scattered by mono-energetic electrons with Lorentz factor γ_i . The factor $x_0 \sim 0.5$ is necessary to ensure energy conservation.

In this section, we assume that only the first-order SSC component is important. When the Klein-Nishina correction can be neglected, Gao et al. (2013) approximate the analytical SSC spectra. Similar to the synchrotron radiation, the SSC spectra is determined by the relationship among ν_a, ν_m and ν_c :

(1) $\nu_a < \nu_m < \nu_c$:

$$F_\nu^{\text{IC}} = \frac{1}{\Omega} \tau_{\text{es}} F_{\nu, \text{max}} x_0 \times \begin{cases} \frac{5}{2} \frac{p-1}{p+1} \left(\frac{\nu_a}{\nu_m}\right)^{\frac{1}{3}} \left(\frac{\nu}{\nu_{ma}^{\text{IC}}}\right) & \nu < \nu_{ma}^{\text{IC}}, \\ \frac{3}{2} \frac{p-1}{p-1/3} \left(\frac{\nu}{\nu_{ma}^{\text{IC}}}\right)^{\frac{1}{3}} & \nu_{ma}^{\text{IC}} < \nu < \nu_{mm}^{\text{IC}}, \\ \frac{p-1}{p+1} \left(\frac{\nu}{\nu_{mm}^{\text{IC}}}\right)^{\frac{1-p}{2}} \left[\frac{4(p+1/3)}{(p+1)(p-1/3)} + \ln\left(\frac{\nu}{\nu_{mm}^{\text{IC}}}\right) \right] & \nu_{mm}^{\text{IC}} < \nu < \nu_{mc}^{\text{IC}}, \\ \frac{p-1}{p+1} \left(\frac{\nu}{\nu_{mm}^{\text{IC}}}\right)^{\frac{1-p}{2}} \left[\frac{2(2p+3)}{p+2} - \frac{2}{(p+1)(p+2)} + \ln\left(\frac{\nu_{cc}^{\text{IC}}}{\nu}\right) \right] & \nu_{mc}^{\text{IC}} < \nu < \nu_{cc}^{\text{IC}}, \\ \frac{p-1}{p+1} \left(\frac{\nu}{\nu_{mm}^{\text{IC}}}\right)^{-\frac{p}{2}} \left(\frac{\nu_c}{\nu_m}\right) \left[\frac{2(2p+3)}{p+2} - \frac{2}{(p+2)^2} + \frac{p+1}{p+2} \ln\left(\frac{\nu}{\nu_{cc}^{\text{IC}}}\right) \right] & \nu_{cc}^{\text{IC}} < \nu. \end{cases} \quad (\text{B16})$$

(2) $\nu_m < \nu_a < \nu_c$:

$$F_\nu^{\text{IC}} = \frac{1}{\Omega} \tau_{\text{es}} F_{\nu, \text{max}} x_0 \times \begin{cases} \frac{2(p+4)(p-1)}{3(p+1)^2} \left(\frac{\nu_m}{\nu_a}\right)^{\frac{p+1}{2}} \left(\frac{\nu}{\nu_{ma}^{\text{IC}}}\right) & \nu < \nu_{ma}^{\text{IC}}, \\ \frac{p-1}{p+1} \left(\frac{\nu}{\nu_{mm}^{\text{IC}}}\right)^{\frac{1-p}{2}} \left[\frac{2(2p+5)}{(p+1)(p+4)} + \ln\left(\frac{\nu}{\nu_{ma}^{\text{IC}}}\right) \right] & \nu_{ma}^{\text{IC}} < \nu < \nu_{mc}^{\text{IC}}, \\ \frac{p-1}{p+1} \left(\frac{\nu}{\nu_{mm}^{\text{IC}}}\right)^{\frac{1-p}{2}} \left[2 + \frac{2}{p+4} + \ln\left(\frac{\nu}{\nu_a}\right) \right] & \nu_{mc}^{\text{IC}} < \nu < \nu_{ca}^{\text{IC}}, \\ \frac{p-1}{p+1} \left(\frac{\nu}{\nu_{mm}^{\text{IC}}}\right)^{\frac{1-p}{2}} \left[\frac{2(2p+1)}{p+1} + \ln\left(\frac{\nu_{cc}^{\text{IC}}}{\nu}\right) \right] & \nu_{ca}^{\text{IC}} < \nu < \nu_{cc}^{\text{IC}}, \\ \frac{p-1}{p+2} \left(\frac{\nu_c}{\nu_m}\right) \left(\frac{\nu}{\nu_{mm}^{\text{IC}}}\right)^{-\frac{p}{2}} \left[\frac{2(2p+5)}{p+2} + \ln\left(\frac{\nu}{\nu_{cc}^{\text{IC}}}\right) \right], & \nu > \nu_{cc}^{\text{IC}}. \end{cases} \quad (\text{B17})$$

(3) $\nu_a < \nu_c < \nu_m$:

$$F_\nu^{\text{IC}} = \frac{1}{\Omega} \tau_{\text{es}} F_{\nu, \text{max}} x_0 \times \begin{cases} \frac{5}{6} \left(\frac{\nu_a}{\nu_c} \right)^{\frac{1}{2}} \left(\frac{\nu}{\nu_{ca}} \right) & \nu < \nu_{ca}^{\text{IC}}, \\ \frac{9}{10} \left(\frac{\nu}{\nu_{cc}^{\text{IC}}} \right)^{\frac{1}{3}} & \nu_{ca}^{\text{IC}} < \nu < \nu_{cc}^{\text{IC}}, \\ \frac{1}{3} \left(\frac{\nu}{\nu_{cc}^{\text{IC}}} \right)^{-\frac{1}{2}} \left[\frac{28}{15} + \ln \left(\frac{\nu}{\nu_{cc}^{\text{IC}}} \right) \right] & \nu_{cc}^{\text{IC}} < \nu < \nu_{cm}^{\text{IC}}, \\ \frac{1}{3} \left(\frac{\nu}{\nu_{cc}^{\text{IC}}} \right)^{-\frac{1}{2}} \left[\frac{2(p+5)}{(p+2)(p-1)} - \frac{2(p-1)}{3(p+2)} + \ln \left(\frac{\nu_{mm}^{\text{IC}}}{\nu} \right) \right] & \nu_{cm}^{\text{IC}} < \nu < \nu_{mm}^{\text{IC}}, \\ \frac{1}{p+2} \left(\frac{\nu_c}{\nu_m} \right) \left(\frac{\nu}{\nu_{mm}^{\text{IC}}} \right)^{-\frac{p}{2}} \left[\frac{2}{3} \frac{p+5}{p-1} - \frac{2}{3} \frac{p-1}{p+2} + \ln \left(\frac{\nu}{\nu_{mm}^{\text{IC}}} \right) \right] & \nu_{mm}^{\text{IC}} < \nu. \end{cases} \quad (\text{B18})$$

(4) $\nu_c < \nu_a < \nu_m$:

$$F_\nu^{\text{IC}} = \frac{1}{\Omega} \tau_{\text{es}} F_{\nu, \text{max}} x_0 \times \begin{cases} \left(\frac{1}{2} \mathcal{R} + 1 \right) (\mathcal{R} + 4) \left(\frac{\nu}{\nu_{aa}^{\text{IC}}} \right) & \nu < \nu_{aa}^{\text{IC}}, \\ \mathcal{R} \left(\frac{\nu}{\nu_{aa}^{\text{IC}}} \right)^{-\frac{1}{2}} \left[\frac{1}{6} \mathcal{R} + \frac{9}{10} + \frac{1}{4} \mathcal{R} \ln \left(\frac{\nu}{\nu_{aa}^{\text{IC}}} \right) \right] & \nu_{aa}^{\text{IC}} < \nu < \nu_{am}^{\text{IC}}, \\ \mathcal{R}^2 \left(\frac{\nu}{\nu_{aa}^{\text{IC}}} \right)^{-\frac{1}{2}} \left[\frac{3}{p-1} - \frac{1}{2} + \frac{3}{4} \ln \left(\frac{\nu_{mm}^{\text{IC}}}{\nu} \right) \right] & \nu_{am}^{\text{IC}} < \nu < \nu_{mm}^{\text{IC}}, \\ \frac{9}{2(p+2)} \mathcal{R}^2 \left(\frac{\nu_a}{\nu_m} \right) \left(\frac{\nu}{\nu_{mm}^{\text{IC}}} \right)^{-\frac{p}{2}} \left[\frac{4}{p+3} \left(\frac{\gamma_a}{\gamma_m} \right)^{p-1} \frac{\gamma_a}{\gamma_c} + \frac{3(p+1)}{(p-1)(p+2)} + \frac{1}{2} \ln \frac{\nu}{\nu_{mm}^{\text{IC}}} \right] & \nu > \nu_{mm}^{\text{IC}}. \end{cases} \quad (\text{B19})$$

(4) $\max(\nu_c, \nu_m) < \nu_a$:

$$F_\nu^{\text{IC}} = \frac{1}{\Omega} \tau_{\text{es}} F_{\nu, \text{max}} x_0 \times \begin{cases} \left(\frac{3\mathcal{R}}{2(p+2)} + 1 \right) \left(\frac{3\mathcal{R}}{p+2} + 4 \right) \left(\frac{\nu}{\nu_{aa}^{\text{IC}}} \right) & \nu < \nu_{aa}^{\text{IC}}, \\ \frac{1}{p+2} \left[\frac{6\mathcal{R}}{p+3} + \mathcal{R} \left(\frac{9\mathcal{R}}{2(p+2)} + 1 \right) + \frac{9\mathcal{R}^2}{4} \ln \left(\frac{\nu}{\nu_{aa}^{\text{IC}}} \right) \right] \left(\frac{\nu}{\nu_{aa}^{\text{IC}}} \right)^{-\frac{p}{2}}, & \nu > \nu_{aa}^{\text{IC}} \end{cases} \quad (\text{B20})$$

Where τ_{es} is the electron scattering optical depth, and \mathcal{R} is the flux ratio between the pile-up peak and the optically thin limit at ν_a .

C. KLEIN-NISHINA CORRECTION

In higher frequency bands, the SSC is suppressed by the Klein-Nishina effect. Therefore, the shape of spectrum should be corrected for both synchrotron and SSC radiation. [Nakar et al. \(2009\)](#) have provided a comprehensive treatment of the Klein-Nishina effect. In this section, we refer to their analysis results of the spectrum.

For convenience, the upper limit of the Lorentz factor of electrons that can effectively scatter photons emitted by electrons with a Lorentz factor of γ_e is defined as ([Nakar et al. 2009](#))

$$\hat{\gamma}_e = \frac{\gamma m_e c^2}{h\nu_e}. \quad (\text{C21})$$

Therefore, we can define the new critical Lorentz factors $\hat{\gamma}_m, \hat{\gamma}_c$ corresponding to ν_m, ν_c . And since Y is correlated with γ_e when the KN effect is significant, a new critical Lorentz factor $\gamma_{e,0}$ can be defined, satisfying $Y(\gamma_{e,0}) = 1$.

For the fast cooling, the spectrum is divided into three situations based on the relationship between γ_m and $\hat{\gamma}_m$. When $\gamma_m < \hat{\gamma}_m$, the spectrum of synchrotron and SCC radiation can be divided into two cases:

(1) $\gamma_0 < \hat{\gamma}_c$:

$$F_\nu^{\text{syn}} \propto \begin{cases} \nu^{-\frac{1}{2}} & \nu_c < \nu < \nu_m, \\ \nu^{-\frac{p}{2}} & \nu_m < \nu < \hat{\nu}_m, \\ \nu^{-(\frac{p}{2}-\frac{1}{4})} & \hat{\nu}_m < \nu < \nu_0, \\ \nu^{-\frac{p}{2}} & \nu_0 < \nu. \end{cases} \quad (\text{C22})$$

$$F_\nu^{\text{IC}} \propto \begin{cases} \nu^{-\frac{p}{2}} & \nu_{mm} < \nu < 2\nu_m \hat{\gamma}_m^2, \\ \nu^{-(p-1)} & 2\nu_m \hat{\gamma}_m^2 < \nu < 2\nu_m \hat{\gamma}_m \gamma_0, \\ \nu^{-(p-\frac{1}{2})} & 2\nu_m \hat{\gamma}_m \gamma_0 < \nu < 2\nu_c \hat{\gamma}_c^2, \\ \nu^{-(p+\frac{1}{3})} & 2\nu_c \hat{\gamma}_c^2 < \nu. \end{cases} \quad (\text{C23})$$

(2) $\gamma_0 > \hat{\gamma}_c$:

$$F_\nu^{\text{syn}} \propto \begin{cases} \nu^{-\frac{1}{2}} & \nu_c < \nu < \nu_m, \\ \nu^{-\frac{p}{2}} & \nu_m < \nu < \hat{\nu}_m, \\ \nu^{-(\frac{p}{2}-\frac{1}{4})} & \hat{\nu}_m < \nu < \hat{\nu}_c, \\ \nu^{-(\frac{p}{2}-\frac{2}{3})} & \hat{\nu}_c < \nu < \nu_0, \\ \nu^{-\frac{p}{2}} & \nu_0 < \nu. \end{cases} \quad (\text{C24})$$

$$F_\nu^{\text{IC}} \propto \begin{cases} \nu^{-\frac{p}{2}} & \nu_m \gamma_m^2 < \nu < \nu_m \hat{\gamma}_m^2, \\ \nu^{-(p-1)} & \nu_m \hat{\gamma}_m^2 < \nu < \nu_m \hat{\gamma}_m \gamma_0, \\ \nu^{-(p+\frac{1}{3})} & \nu_m \hat{\gamma}_m \gamma_0 < \nu. \end{cases} \quad (\text{C25})$$

However, when $p \approx 2$, another power-law segment is added to the synchrotron spectrum for the case with $\hat{\gamma}_c < \gamma_0$: $F_\nu^{\text{syn}} \propto \nu^{-3/8}$ for $\max(\nu_c, \hat{\nu}_0) < \nu < \hat{\nu}_m$.

When $\gamma_m > \hat{\gamma}_m$, the spectrum is divided into three cases. In each case, the spectrum of the SSC radiation is too complex to describe with precise power-law segments (Nakar et al. 2009). However, the power-law indices of the various segments are typically similar (the difference is $\leq 1/4$). Therefore, The spectrum can be described approximately.

(1) $\frac{\epsilon_e}{\epsilon_B} < \left(\frac{\gamma_m}{\hat{\gamma}_m}\right)^{\frac{1}{3}}$

$$F_\nu^{\text{syn}} \propto \begin{cases} \nu^{-\frac{1}{2}} & \nu_c < \nu < \hat{\nu}_m, \\ \nu^{-\frac{1}{4}} & \hat{\nu}_m < \nu < \nu_0, \\ \nu^{-\frac{1}{2}} & \nu_0 < \nu < \nu_m, \\ \nu^{-\frac{p}{2}} & \nu_m < \nu. \end{cases} \quad (\text{C26})$$

For SSC radiation, the peak of νF_ν^{IC} is at $2\nu_m \gamma_m \hat{\gamma}_m$. When the frequencies are much lower than peak frequency, the power-law index of F_ν^{IC} is $1/4$. At frequencies close to the peak but still below the peak frequency, the index can be between $-3/4$ and $-1/2$. At frequencies are higher than the peak frequency, the power-law index ranges between $-p + 1/4$ and $-p + 1/2$, until $\nu > 2\nu_c \hat{\gamma}_c^2$, where the power-law index becomes $-p - 1/3$.

(2) $\left(\frac{\gamma_m}{\hat{\gamma}_m}\right)^{\frac{1}{3}} < \frac{\epsilon_e}{\epsilon_B} < \frac{\gamma_m}{\hat{\gamma}_m}$

$$F_\nu^{\text{syn}} \propto \begin{cases} \nu^{-\frac{1}{2}} & \nu_c < \nu < \hat{\nu}_m, \\ \nu^{-\frac{1}{4}} & \hat{\nu}_m < \nu < \hat{\nu}_0, \\ \nu^0 & \hat{\nu}_0 < \nu < \nu_0, \\ \nu^{-\frac{1}{2}} & \nu_0 < \nu < \nu_m, \\ \nu^{-\frac{p}{2}} & \nu_m < \nu. \end{cases} \quad (\text{C27})$$

For SSC, at frequencies are just lower than peak frequency ($2\nu_m \gamma_m \hat{\gamma}_m$), the power-law index is $-3/4$. When the frequencies are lower than $\sqrt{\frac{\hat{\gamma}_m \epsilon_e}{\gamma_m \epsilon_B}} 2\nu_m \gamma_m \hat{\gamma}_m$, the power-law index becomes $-1/4$. When the frequencies are just higher than peak frequency, the power-law index is between $-p$ and $-p + 1/4$. At even higher frequencies, the power-law index is $-p + 1/2$. When the frequency reaches $2\nu_c \hat{\gamma}_c^2$ and the power-law index becomes $-p - 1/3$.

(3) $\frac{\gamma_m}{\hat{\gamma}_m} < \frac{\epsilon_e}{\epsilon_B} < \left(\frac{\gamma_m}{\hat{\gamma}_m}\right)^3$

$$F_\nu^{\text{syn}} \propto \begin{cases} \nu^{-\frac{1}{2}} & \nu_c < \nu < \hat{\nu}_0, \\ \nu^{-\frac{p-1}{4}} & \hat{\nu}_0 < \nu < \hat{\nu}_m, \\ \nu^0 & \hat{\nu}_m < \nu < \nu_m, \\ \nu^{-\frac{p-1}{2}} & \nu_m < \nu < \nu_0, \\ \nu^{-\frac{p}{2}} & \nu_0 < \nu. \end{cases} \quad (\text{C28})$$

For SSC, the peak frequency of νF_ν^{IC} is $\nu_m \gamma_m \hat{\gamma}_m$. When the frequencies are lower than the peak frequency, the range of power-law index is from $-1/4$ to 0 . And the frequencies are higher than the peak frequency, the range of power-law index is from $-p$ to $-p + 1/2$. If the frequencies are higher than $2\nu_c \hat{\gamma}_c^2$, the power-law index is $-p - 1/3$.

There is an another case for $\gamma_m = \hat{\gamma}_m$. In this case, the spectrum is divided into 2 cases by $p = 2.5$. If $p < 2.5$, the synchrotron spectrum is

$$F_\nu^{\text{syn}} \propto \begin{cases} \nu^{-\frac{1}{2}} & \nu_c < \nu < \hat{\nu}_0, \\ \nu^{-\frac{p-1}{3}} & \hat{\nu}_0 < \nu < \nu_m, \\ \nu^{-\frac{2(p-1)}{3}} & \nu_m < \nu < \nu_0, \\ \nu^{-\frac{p}{2}} & \nu_0 < \nu. \end{cases} \quad (\text{C29})$$

And the SSC spectrum is

$$F_\nu^{\text{IC}} \propto \begin{cases} \nu^{-\frac{1}{2}} & \nu_{cm} < \nu < 2\nu_m \hat{\gamma}_0^2, \\ \nu^{-\frac{p-1}{3}} & 2\nu_m \hat{\gamma}_0^2 < \nu < \nu_{mm}, \\ \nu^{-p+1} & \nu_{mm} < \nu < 2\nu_m \gamma_m \gamma_0, \\ \nu^{-\frac{2p+1}{3}} & 2\nu_m \gamma_m \gamma_0 < \nu < 2\nu_m \gamma_m \hat{\gamma}_0, \\ \nu^{-p+\frac{1}{2}} & 2\nu_m \gamma_m \hat{\gamma}_0 < \nu. \end{cases} \quad (\text{C30})$$

When $p > 2.5$, for the spectrum of synchrotron, the power-law index between ν_c and ν_m is modified to $-1/2$. And at $\nu_m < \nu < \nu_0$, the power-law index is modified to $-p/2 + 1/4$. For the SSC spectrum, the power-law index between ν_{cc} and ν_{mm} is modified to $-1/2$. And at $2\nu_m \gamma_m \gamma_0 < \nu$, the power-law index is modified to $-p + 1/2$.

For the slow cooling, the synchrotron spectrum above ν_c is

$$F_\nu^{\text{syn}} \propto \begin{cases} \nu^{-\frac{p}{2}} & \nu_c < \nu < \hat{\nu}_c, \\ \nu^{-\frac{3}{4}(p-1)} & \max(\hat{\nu}_c, \nu_c) < \nu < \min(\hat{\nu}_m, \nu_0), \\ \nu^{-\left(\frac{p}{2} - \frac{2}{3}\right)} & \hat{\nu}_m < \nu < \nu_0, \\ \nu^{-\frac{p}{2}} & \nu_0 < \nu. \end{cases} \quad (\text{C31})$$

And the spectrum of SSC radiation is

$$F_\nu^{\text{IC}} \propto \begin{cases} \nu^{-\frac{p}{2}} & \nu_{cc} < \nu < 2\nu_c \hat{\gamma}_c^2, \\ \nu^{-(p-1)} & 2\nu_c \hat{\gamma}_c \max(\hat{\gamma}_c, \gamma_c) < \nu < 2\nu_c \hat{\gamma}_c \min(\gamma_0, \hat{\gamma}_m), \\ \nu^{-\frac{p+1}{2}} & 2\nu_c \hat{\gamma}_c \gamma_0 < \nu < 2\nu_c \hat{\gamma}_c \hat{\gamma}_m, \\ \nu^{-(p+\frac{1}{3})} & 2\nu_c \hat{\gamma}_c \max(\gamma_0, \hat{\gamma}_m) < \nu. \end{cases} \quad (\text{C32})$$

It's worth noting that, for both synchrotron and SSC spectrum, not all these segments can be observed for all cases. For example, the first segment of synchrotron and SSC can be observed only at $\gamma_c < \hat{\gamma}_c$. And the third segment of synchrotron can be observed only at $\hat{\gamma}_m < \gamma_0$. But in this case, the third segment of SSC can't be observed.